Influence of circular RNA topology on microRNA stability

Federico Fuchs Wightman[1, 2*], Jerónimo Lukin[3*], Sebastián Giusti[3], Michael Soutschek[4, 5], Laureano Bragado[1, 2], Berta Pozzi[6], Paula González[7], Juan P. Fededa[7], Gerhard Schratt[4, 5], Damián Refojo[3#] & Manuel de la Mata[2, 8#]

[1]Universidad de Buenos Aires, Facultad de Ciencias Exactas y Naturales.

[2]CONICET-Universidad de Buenos Aires, Instituto de Fisiología, Biología Molecular y Neurociencias (IFIBYNE), Buenos Aires, Argentina.

[3]Instituto de Investigación en Biomedicina de Buenos Aires (IBioBA) - CONICET - Partner Institute of the Max Planck Society, Godoy Cruz 2390, C1425FQD Buenos Aires, Argentina.

[4]Lab of Systems Neuroscience, D-HEST Institute for Neuroscience, ETH Zürich, Switzerland.

[5]Neuroscience Center Zurich, ETH Zurich and University of Zurich, Switzerland.

[6]Institute of Cell Biology, University of Bern, Bern, Switzerland.

[7]Instituto de Investigaciones Biotecnológicas "Dr. Rodolfo A. Ugalde", IIB-UNSAM, IIBIO-CONICET, Universidad Nacional de San Martín, Buenos Aires, Argentina.

[8]Universidad de Buenos Aires, Facultad de Ciencias Exactas y Naturales. Departamento de Fisiología, Biología Molecular y Celular.

[*]Contributed equally.

[#]Correspondence: drefojo@ibioba-mpsp-conicet.gov.ar, mmata@fbmc.fcen.uba.ar.

Abstract

Circular RNAs (circRNAs) have been proposed to “sponge” or block microRNAs, a property shared with linear RNAs. Alternatively, certain RNAs induce microRNA destruction through the process of Target RNA-Directed MicroRNA Degradation (TDMD). Whether both linear and circular transcripts are equivalent in driving TDMD is unknown. Here we show that RNA topology seems critical for TDMD. Through a novel system that expresses a circRNA while reducing the co-expressed cognate linear RNA, we propose that circRNAs cannot induce TDMD. Interestingly, this appears attributed to the circular

RNA topology and not to its sequence, which is TDMD-competent in its linear form. Similarly, based on the previous knowledge that *Cdr1as* circular RNA protects miR-7 from Cyrano-mediated TDMD, we demonstrate that depletion of *Cdr1as* reduces miR-7 abundance, while overexpression of an artificial linear version of *Cdr1as* drives TDMD. By analysing RNA sequencing data of a neuron differentiation system, we detect potential events of circRNA-mediated microRNA stabilization. Our results support a model in which circRNAs, unlike linear mRNAs, lead to a topology-dependent TDMD evasion, aiding in the stabilization of specific microRNAs.

Keywords: circRNA/microRNA/TDMD

Introduction

Circular RNAs (circRNAs) are long known regulatory RNAs that have gained remarkable attention since the first reports that highlighted their high diversity and abundance (Memczak *et al*, 2013; Hansen *et al*, 2013; Salzman *et al*, 2013; Jeck *et al*, 2013). CircRNAs are covalently closed structures that originate from pre-mRNA backsplicing and therefore lack a poly-A tail and 5'-cap. As a result, given that these terminal modifications are the entry points for the microRNA (miRNA) effector machinery (Bartel, 2018; Jonas & Izaurralde, 2015), circRNAs seem largely immune to posttranscriptional degradation by miRNAs. Conversely, although current knowledge points towards a diversity of both nuclear and cytoplasmic functions for different individual circRNAs, several findings have suggested that some circRNAs regulate gene expression by working as miRNA "sponges" (Chen, 2020; Xiao *et al*, 2020; Hanan *et al*, 2020).

Whether circRNAs act on miRNAs by blocking them functionally, affecting their stability, or a combination of both remains to be determined. In particular, it is unclear whether circRNAs are active in driving Target Directed MicroRNA Degradation (TDMD), a mechanism that has emerged as central in affecting miRNA turnover. During TDMD, targets with extensive base-pair complementarity towards the 3' end of the miRNA –i.e. displaying no more than 3 mismatches in addition to a central bulge– lead to miRNA degradation, reversing the logic of canonical miRNA target silencing by which the target RNA is conventionally degraded (Ameres *et al*, 2010; Cazalla *et al*, 2010; Marcinowski *et al*, 2012; Fuchs Wightman *et al*, 2018). TDMD induces a conformational change on Argonaute (AGO) proteins that leads to their poly-ubiquitination and degradation, rendering the specifically loaded miRNAs unprotected

and susceptible to degradation by general nucleases (Shi *et al*, 2020; Han *et al*, 2020). Unlike sponging, TDMD-inducing targets act catalytically even at sub-stoichiometric levels, resulting in the most selective and potent miRNA degradation mechanism described to date and which seems to explain the half-lives of most naturally unstable miRNAs (de la Mata *et al*, 2015; Denzler *et al*, 2016; Kleaveland *et al*, 2018; Shi *et al*, 2020). A priori, the circular topology of circRNAs should not represent an impediment to regulating miRNAs through TDMD, and circRNAs' high stability could even be an advantage for this activity. Nevertheless, to date no circRNA has been described to drive TDMD and the only available evidence indicates that circRNAs might instead lead to miRNA stabilization (Piwecka *et al*, 2017; Chen *et al*, 2019).

CircRNAs are typically coexpressed with their cognate linear RNAs from the common host genes. However, the circRNA over linear ratio occurs in different proportions, with a subset of circRNAs reaching higher levels than their cognate linear isoforms (Chen, 2020). To reveal insights into circRNA-specific functions and mechanisms, a plethora of publications have relied on circRNA overexpression using various inverted repeat-containing vectors (Zhang *et al*, 2014; Conn *et al*, 2015; Liang & Wilusz, 2014; Kramer *et al*, 2015; Li *et al*, 2017, 90; Liu *et al*, 2019; Guarnerio *et al*, 2019; Litke & Jaffrey, 2019; Memczak *et al*, 2013; Hansen *et al*, 2013). Yet, the capability of plasmid-based methods to overexpress exogenous circRNAs free from overlapping, "leaky" linear RNA expression remains questionable. Thus, attributing any observed effects to the overexpressed circRNA while not rigorously controlling for the potential role of the undesired coexpressed linear transcripts represents a potential pitfall (Pamudurti *et al*, 2017; Kristensen *et al*, 2019; Dodbele *et al*, 2021; Chen, 2020).

A key general question in the field that remains largely unanswered, is whether the circular nature of circRNAs is intrinsically or mechanistically linked to their molecular functions. In this study we aimed to elucidate whether linear and circular target topologies function differently to affect miRNA stability and function. Using a strategy that allows us to express an artificial circRNA with reduced expression of the counterpart linear transcript, we showed that the circular RNA, as opposed to the linear form, seems unable to induce TDMD. We also examined the well described *Cdr1as*-miR-7-Cyrano network of noncoding RNAs, where the lncRNA Cyrano destabilizes miR-7-5p through TDMD (Kleaveland *et al*, 2018), while the circRNA CDR1as (also known as ciRS-7) yields a protection on miR-7-5p (Piwecka *et al*, 2017). We show that expression of an artificially linear version of *Cdr1as* triggers TDMD and is unable to rescue the endogenous circRNA loss of function, suggesting that the circular topology of *Cdr1as* is

crucial for the evasion of TDMD. Finally, we show that certain circRNA-miRNA interactions might lead to a phenomenon of miRNA stabilization, representing a potentially active mechanism during neuron-like differentiation.

Results

Artificial circRNA expression

In order to compare the effect of circular and linear RNAs on microRNA stability, we designed constructs capable of expressing either linear transcripts or artificial circRNAs encompassing segments of identical primary sequence (Figure 1A). Both the linear and circular RNAs contain 4 binding sites for a candidate miRNA (miR-132) with proven TDMD-competent sequence complementarity (de la Mata *et al*, 2015) (Figure EV1A). To express the circRNA, we followed a strategy consisting of inserting acceptor and donor splice sites flanking the segment of the transcript to be circularized, plus Alu reverse complementary sequences (RCS) from the introns of a naturally circularized RNA (human ZKSCAN1 exons 2 and 3 respectively), (Figure 1A) (Liang & Wilusz, 2014). In order to preferentially enrich the expression of the circular over the linear variant in neurons, we introduced perfectly matched sites against a highly expressed neuron-specific miRNA (miR-124) which are lost after RNA processing in the backspliced circular product but remain present in the linear RNA isoform, thus rendering the linear – but not the circular– RNA form susceptible to AGO2 slicing (Figure 1A). As a TDMD positive control, we expressed a linear transcript with identical sequence to the circRNA-expressing construct, but lacking the splice sites and the reverse complementary flanking introns that induce circularization (Liang & Wilusz, 2014) (Figures 1A and EV1A). The latter constructs have been proved effective in triggering TDMD in primary neurons (de la Mata *et al*, 2015). All constructs were packed into lentiviral vectors and used to transduce mouse primary neurons.

To control the miRNA-mediated degradation of the linear byproduct, we generated two circRNA expressing constructs, differing by seed-mutations in the miR-124 binding sites (Figure EV1A). We first sought to validate that the constructs expressed a single circRNA species with covalently linked ends and no concatemers or other spurious by-products, by performing Northern blot analysis of RNase R treated or untreated samples from HEK293T cells –a cell line where miR-124 is not endogenously expressed. We observed that both circRNA-expressing constructs bearing either perfect or seed-mutant

sites for miR-124, produced two bands: a single RNase R-resistant circRNA product and an RNase R-sensitive linear RNA form. The fact that the artificial circRNA was not susceptible to the RNase R digestion relative to the linear transcript, supports a circular structure (Figure EV1B and D). Importantly, digital quantification of northern blot bands correlated strictly with the RT-qPCR measurements using primers to amplify either the circular isoform exclusively (Figure 1A, primer pair #1) or both the linear and circular isoforms combined –hereafter referred to as Total Output (TO)– (Figure 1A, primer pair #2), further validating the latter method for subsequent analysis (Figure EV1C). Next, to rule out artifacts that could be caused by template switching during cDNA synthesis and that could serve as templates for the divergent primers -designed to amplify across the artificial circRNA backspliced junction- (Figure 1A, primer pair #1), we performed the PCR from cDNAs obtained with two different reverse transcriptases (MMLV-RT & Superscript II). Amplification from both cDNAs produced identical PCR products with identical sequences spanning the predicted backsplicing junction (Figure EV1E). Because the two RT enzymes are unlikely to jump at the exact same sequences during a putative template switching event, we conclude the transcripts produced from our expression system are bona fide circRNAs.

In order to quantify the linear/circular RNA ratio produced by our circRNA-expressing constructs, the relative intensities of the bands were acquired by densitometry using Image J. On average, the linear/circular RNA ratio obtained was in the order of 4±1 in HEK293T cells (Figure EV1B), a cell line that does not express miR-124 and therefore does not degrade the linear RNA. To validate that our strategy was successful at expressing a circRNA while selectively degrading its counterpart linear transcript by means of miR-124, we transduced the circRNA-expressing constructs into mouse primary neurons and performed RT-qPCR using both the primers described above plus additional primers to amplify the linear isoform exclusively (Figure 1A, primer pair #3). Remarkably, we observed that our strategy led to a potent (3-4 fold) degradation of "leak" linear RNA without affecting circRNA abundance (Figure 1B). Furthermore, circRNA levels produced from the circRNA-expressing construct were exceedingly higher than from the construct expressing the linear RNA (TDMD inducer), with both constructs producing equivalent total output levels (Figure 1C). Altogether, these results confirm that our system is effective in expressing circRNAs while reducing the abundance of their cognate linear RNAs, making it a generally useful tool in experiments aimed at dissecting circRNA function.

CircRNA-expressing construct is incapable of triggering TDMD

To explore whether linear and circular target topologies function differently to affect miRNA stability through TDMD, we determined the extent to which a circular RNA topology can impact miRNA stability via TDMD in neurons, a cell type known to display a potent TDMD effect (de la Mata *et al*, 2015). To this end we transduced primary neurons with either linear or circRNA expression constructs bearing TDMD-competent (bulged) or seed-mutant binding sites for miR-132, and measured miR-132 abundance by an RT-qPCR Taqman assay. Whereas the linear TDMD inducer was capable of effectively destabilizing miR-132, the circRNA-expressing construct showed no effect on miRNA stability. Considering that the circRNA-expressing construct reduces the linear RNA abundance by 3-4 fold in neurons and that the TO of the circRNA-expressing construct remains similar to that of the linear RNA-only expressing construct (TDMD inducer), we conclude that: 1) the circRNA levels account for up to 30-50% of the total RNA abundance expressed from the circRNA-expressing construct in neurons (compared to the ca. 25% in HEK293T cells that lack endogenous miR-124), and 2) the fact that no miR-132 downregulation is observed under these conditions suggests that up to the extent that we were able to express the artificial circRNA, it appears unable to contribute to any additional TDMD effect, and it likely even antagonizes the TDMD effect driven by its co-expressed linear counterpart. (Figures 1C and 2A). We confirmed that miR-132 downregulation by the linear TDMD inducer was not a consequence of changes in transcription and/or maturation of the targeted miRNA by showing that the abundance of the primary transcript (pri-miR-132) and passenger strand (miR-132-5p) of miR-132 remained unchanged, confirming that the reduction in the miR-132 guide strand was a bona fide post-transcriptional effect occurring after miR-132 processing and therefore consistent with TDMD (Figure EV2A). To control for the specificity of the linear TDMD inducer against miR-132, we measured the levels of four (4) additional control mature miRNAs (miR-124, -128, -138 and -409). None of them were significantly affected, confirming that the effect is indeed specific for miR-132 (Figure EV2A).

In order to determine whether the observed differential effect could be attributed to the inability of the circular RNA to bind to the RISC complex, we set out an RNA immunoprecipitation experiment (RIP) by specifically pulling-down AGO2 and isolating all copurifying RNA species. To this end, we co-transfected HEK293T cells with FLAG/HA-AGO2 together with the different circRNA-expressing

constructs and a vector for pri-miR-132 (otherwise of low abundance in HEK293T cells) followed by immunoprecipitation and RT-qPCR analysis. We observed that the artificial circRNA was effectively pulled down together with AGO2 only when carrying bulged sites for miR-132 but not if the sites were mutated at the miRNA seed-binding region (Figures 2B and EV2B-C). These results demonstrate that the circular RNA is indeed able to specifically bind to the RISC complex, ruling out that defects in circRNA-AGO2 binding could account for the observed lack of TDMD activity.

To exclude the possibility that the observed differences were a trivial consequence of an aberrant localization of the circRNA relative to the linear isoform (Chen, 2020), we performed a purification of nuclear and cytoplasmic subcellular fractions. Our results showed that the artificial circRNA accumulates in the cytoplasm at similar proportions relative to the linear control and is only slightly lower in the nuclear compartment (Figures 2C and EV2D-E), suggesting that the inability of the circRNA to trigger TDMD is not related to it being retained in the nucleus.

Circular topology of *Cdr1as* is necessary to protect miR-7 from TDMD

To answer whether the inability to trigger TDMD was restricted to our circRNA expression system or if it may actually be observed for other known endogenous circRNAs as well, we studied the case of the *Cdr1as*-miR-7 interaction (Hansen *et al*, 2011, 2013; Memczak *et al*, 2013). To determine whether the circular topology of *Cdr1as* has a role in modulating miR-7 abundance, we designed tools to manipulate endogenous *Cdr1as* levels in rodent primary neurons (Fellmann *et al*, 2013). In order to knock down *Cdr1as* we engineered a lentiviral vector to express a specific shRNAmiR (sh*Cdr1as*) (Figure EV3A) and transduced it in primary neurons at high efficiency. Interestingly, the effective *Cdr1as* knockdown achieved did not increase miR-7 levels as expected had *Cdr1as* been an active inducer of TDMD on this miRNA. On the contrary, and in line with previous evidence (Piwecka *et al*, 2017), *Cdr1as* knockdown reduced miR-7 levels, consistent with a stabilization role of the circRNA on this miRNA (Figure 3A-B).

To determine whether the observed effect was dependent on *Cdr1as*'s circular topology, we attempted to rescue the *Cdr1as* knockdown with the expression of an artificial linear version of *Cdr1as* –lin*Cdr1as*– lacking the sh*Cdr1as* target site. Interestingly, the drop of miR-7 abundance caused by the knockdown of the endogenous *Cdr1as*, could be neither rescued nor enhanced by co-expressing the linear *Cdr1as*, even though the artificial lin*Cdr1as* reached expressions levels similar to those of

endogenous *Cdr1as* in control cells (Figure 3A-B). Remarkably, expressing lin*Cdr1as* alone –without knocking down endogenous *Cdr1as*– caused a significant destabilization of miR-7 (Figure 3C-D), consistent with TDMD being driven by the RNA expressed under an artificial linear RNA topology. Importantly, the linear lin*Cdr1as* did not induce a significant variation of the endogenous abundance of (circular) *Cdr1as* (Figure EV3C). To exclude the possibility that miR-7 downregulation was a consequence of changes in transcription and/or maturation of the targeted miRNA upon transduction of lin*Cdr1as*, we measured the abundance of the primary transcript (pri-miR-7a-1), miR-7 passenger strands (miR-7a-1-3p and miR-7a-2-3p) and two (2) additional control miRNAs (miR-9 and -132). Our result shows that the guide strand miR-7-5p, but neither the passenger strands nor the other control miRNAs, undergo degradation by the linear version of Cdr1as (Figure 3D, EV3D). This result confirms that the reduction in the miR-7 is a post-transcriptional effect occurring after miRNA processing and is therefore compatible with active TDMD triggered by the linCdr1as construct (EV3D). Careful inspection of the miR-7 sites present in *Cdr1as* showed that no less than 3 of them indeed exhibit a base pairing complementarity compatible with a TDMD-competent architecture (Figure EV3B) (Fuchs Wightman *et al*, 2018).

As an orthogonal strategy to reduce *Cdr1as* levels and rule out potential off target or indirect effects caused by the sh*Cdr1as*, we used CRISPR/Cas9 genome editing to mutate the splicing sites of the endogenous *Cdr1as* gene. To that end we expressed two sgRNAs against both donor and acceptor splice sites of *Cdr1as* respectively (Figure EV3E). Despite an overall lower efficacy in *Cdr1as* knockdown reached through CRISPR/Cas9 editing compared to the sh*Cdr1as*, we observed a similar effect consistent with *Cdr1as* being unable to induce TDMD on miR-7 but rather leading to its stabilization (Figure EV3E-G).

Overall, our results show that endogenous *Cdr1as* is unable to trigger TDMD on miR-7 but rather stabilizes this miRNA. Accordingly, only if expressed as an artificially linear RNA can it engage in miR-7 degradation through TDMD, further supporting the notion that the natural circular/linear topology, and not just the linear sequence of a RNA target, is a crucial determinant for engaging in such type of regulation.

CircRNAs potentially stabilize dozens of microRNAs across neuron-like differentiation

Based on our results, we hypothesized that circRNAs might possess the ability to influence miRNA stability through evading TDMD and eventually protecting miRNAs from degradation. Yet, whether this type of regulation could be a widespread phenomenon is unclear. To explore this possibility, we analysed available sequencing data of miRNA, circRNA and mRNA expression from hESC H9 cells both undifferentiated and differentiated into forebrain (FB) neuron progenitor cells (Chen *et al*, 2015; Zhang *et al*, 2016). We reasoned that this model would be appropriate to test our hypothesis from the viewpoint that a significant proportion of circRNAs are regulated along neuron differentiation –with upregulation being more frequent than downregulation (You *et al*, 2015; Rybak-Wolf *et al*, 2015). Concomitantly, neuron-specific miRNAs are known to become more susceptible to degradation in more mature neurons (Krol *et al*, 2010), a scenario where circRNAs could act by selectively regulating miRNA stability. In order to consider only the biochemically supported circRNA-miRNA pairs, we used the CLIP-Seq experimentally supported mRNA-miRNA, lncRNA-miRNA and circRNA-miRNA interaction networks catalogued in the STARBASE v3/ENCORI database (Yang *et al*, 2011; Li *et al*, 2014) as a proxy for bona fide interactions.

We first followed a miRNA perspective approach aimed at analysing whether the abundance of miRNAs across the neuron-like differentiation was dependent on the extent of "sponging" imposed by circRNAs. To that end, we initially computed the total number of specific miRNA sites contributed by all circRNAs weighed by circRNA levels before differentiation (hereafter referred to as "miRNA-specific effective sites", see materials and methods and Dataset EV1). We observed that miRNA fold changes across differentiation show no apparent correlation with the number of miRNA-specific effective sites on all circRNAs (Figure 4A). In order to obtain a stoichiometrically relevant estimate of the "sponging suffered" by each miRNA at the onset of differentiation, we further weighted the miRNA-specific effective sites to each miRNA's abundance before differentiation (Figure 4B, ranked in Dataset EV1). According to this analysis, the most highly "sponged" miRNAs, corresponding to those potentially interacting with multiple and/or highly expressed circRNAs at higher circRNA:miRNA stoichiometries early during differentiation, are significantly upregulated across differentiation relative to the least "sponged" miRNAs (Figure 4B-C). We next searched for additional evidence in support of a stabilizing effect of circRNAs which, by acting on top of transcriptional effects, could account for the observed differences in mature miRNA fold changes between the different sponging quartiles. To that end we

estimated the change in pri-miRNA abundance as a proxy for change in transcription levels of the respective miRNA genes across differentiation. Interestingly, while we observe a positive correlation between mature miRNA and pri-miRNA fold changes, the correlation becomes weaker for the most highly "sponged" than for the least "sponged" miRNAs (Figure 4D). By fitting the data to a multiple regression model with interaction, we found that the fold change in mature miRNA levels for the more highly sponged miRNAs (quartile "+++ sponged") seems differentially dependent on the fold change of pri-miRNA levels relative to the least sponged miRNAs (quartile "- sponged") (i.e., the slope changes by ≈2 fold, p-value for the interaction term = 0.0354) (Figure 4D). While this analysis shows that changes in mature miRNA levels are to a large extent explained by changes in transcription of their host genes, the impaired correlation and difference in slope observed for miRNAs in the most highly sponged quartile are consistent with a stabilization effect that cannot be solely explained by changes in their transcription rates. In sum, although we cannot rule out that the more highly upregulated miRNAs are more efficiently processed from their pri-miRNAs than the less upregulated ones, our analysis argues for a post-transcriptional effect of circRNAs on miRNA stability acting in parallel to –but independently of– changes in miRNA transcription. This effect would occur through the concerted interaction of individual miRNAs with multiple and/or highly expressed circRNAs across differentiation.

As a complementary approach from a circRNA perspective, we asked whether the extent of "sponging capacity" offered by circRNAs, namely their ability to simultaneously interact with different miRNAs across differentiation, could impact their own abundance. To that end we calculated a "sponging capacity" index based on the total number of sites (for all miRNAs) present on each circRNA weighed by circRNA levels before differentiation (see materials and methods and Dataset EV1). Interestingly, we observed that an increasing "sponging capacity" index did not correlate with a visible change in circRNA fold changes across differentiation, which is consistent with the notion that circRNAs are not subjected to regulation by miRNAs (Figure 4E). The collection of miRNAs and circRNAs interacting across this neuron-like differentiation might include more than a hundred miRNAs and dozens of circRNAs. In fact, by focusing on the predicted most highly sponging circRNAs, this analysis illustrates that circRNAs with the highest "sponging capacity" for miRNAs lie at highly connected nodes within a complex network, further supporting the view that some individual circRNAs might act as potential scaffolds for multiple miRNAs (Figure EV4A).

Predicted binding of miRNAs to circRNAs through TDMD-like interactions

In order to determine the existence of possible associations between specific features of circRNAs and their ability to engage in potential miRNA-stabilizing interactions, we performed the following analyses. We first compared the median length of circRNAs engaged in interactions with miRNAs subjected to different degrees of sponging by circRNAs. We observed no association between the circRNA median lengths and the degree of sponging (Figure EV4C). We next analysed the genomic regions within transcripts that generate the circRNAs with predicted binding sites for miRNAs of different sponging quartiles. Considering that most circRNAs are expressed from protein coding genes (Guo *et al*, 2014), we analysed the overlapping genomic regions (CDS, 5'UTR, 3'UTR, etc) from such genes only. We observed that the genomic region from which circRNAs originate does not correlate with the degree of miRNA sponging they engage with across differentiation (Figure EV4D).

Our previous knowledge that a limiting number of bona fide TDMD sites –present even at sub-stoichiometric levels– can act catalytically to outcompete the tens of thousands of miRNA binding sites present in the transcriptome (de la Mata *et al*, 2015; Denzler *et al*, 2016; Kleaveland *et al*, 2018; Shi *et al*, 2020) might seem at odds with the interpretation arising from our results that those TDMD sites can be nevertheless antagonized by a few thousand binding sites present on circRNAs. Conceivably, this conundrum could be explained if the miRNA-stabilizing interactions involved sites on circRNAs with TDMD-like architecture themselves. In this scenario, combined with their ability to avoid TDMD, circRNAs bearing TDMD-like sites would act as more effective competitors against bona fide TDMD sites than linear RNAs bearing canonical miRNA sites. To test this hypothesis, we searched for TDMD-like architectures within both circRNAs and 3' UTRs of linear mRNAs using a TDMD-site prediction tool (Soutschek *et al*, 2022). According to this analysis, the most highly "sponged" miRNAs are predicted to interact through TDMD-like interactions with both linear and circRNA at a higher proportion than the least sponged miRNAs, with the proportion of interactions involving circRNAs being overrepresented. From this analysis we conclude that TDMD-like sites on circRNAs may be particularly effective in competing for – and thus stabilizing– miRNAs across differentiation (Figure 5A-B and EV5).

Discussion

A long-lasting and largely unresolved question in the field is whether circRNAs' topology –i.e., their circular nature– is intrinsically relevant for them to exert their molecular actions. Alternatively, the circular form of some circRNAs might have been evolutionarily selected merely based on their resistance to endonucleases that confer them special stability properties. Due to different technical reasons, many of which are related to the expression systems employed, these key questions have not been fully addressed so far.

While most experimental approaches have largely relied on knocking down or overexpressing circRNAs in different organisms or cultured cells, undesirable artifacts can very commonly act as confounding factors in the interpretation of the results. In particular, overexpression of circRNAs suffers from a major caveat related to the unwanted linear RNA species that are inevitably co-expressed from the commonly used expression vectors. This type of problem can easily lead to conclusions where functions are wrongly assigned to circRNAs under circumstances where the associated linear transcripts are the true functional molecules but are ignored in the experiments (Dodbele *et al*, 2021). We have addressed this issue by designing a strategy that allows us to express circRNAs while keeping expression of the counterpart linear product to a minimum. A similar strategy was previously reported in a different context with the goal of restricting expression of transgenes to specific tissues (Brown *et al*, 2007). In our hands the approach proved to work as an efficient tool to deliver high levels of circRNAs while limiting the expression of the linear RNA derived from the circRNA construct (Figure 1).

We have exploited this tool to gain insight into the mechanism of the well-known role of circRNAs in blocking miRNAs. Despite being neither prevalent nor unique to circRNAs as a class, the capacity to inhibit or "sponge" miRNA silencing activity has been the most extensively documented function of circRNAs (Chen, 2020; Dodbele *et al*, 2021). This abundance of papers likely obeys to historical reasons, namely the fact that this was the first function to be reported for circRNAs since their rediscovery during the last decade (Memczak *et al*, 2013; Hansen *et al*, 2013). In spite of this, a clear picture of the mechanism by which some circRNAs act on miRNAs is still missing. For instance, it remains unclear whether circRNAs act on miRNAs simply by blocking their function and/or by affecting their stability. In this sense, although it has been speculated that circRNAs might trigger TDMD like linear RNAs, this premise was never formally and experimentally tested so far (Gasparini *et al*, 2020). Our data suggest the opposite: even when expressed at comparable levels, artificial circular RNAs of identical sequence

to those of TDMD-inducing linear RNAs, prove incapable of inducing TDMD (Figure 2). This is largely recapitulated by the endogenous circRNA *Cdr1as* which cannot trigger TDMD on miR-7 –in fact it leads to its stabilization as discussed below– unless artificially expressed as a linear RNA.

The fact that the protection of miR-7 exerted by *Cdr1as* was not recapitulated by our artificial circRNA on miR-132, might be explained by the still partially present expression of the linear counterpart containing TDMD-active miR-132 sites. An alternative explanation might be the emergent properties of the *Cdr1as*-miR-7-Cyrano network. Based on the latter idea, the stabilization of miR-7 might emerge from the inability of *Cdr1as* to drive TDMD in combination with its preserved ability to bind and compete for miR-7, ultimately shielding the exceptionally potent TDMD activity driven by Cyrano on miR-7 (Kleaveland *et al*, 2018). A similar reasoning might apply to the fact that the artificial (linear) lin*Cdr1as*, when expressed in combination with the knockdown of endogenous (circular) *Cdr1as*, does not produce any additional reduction of miR-7 abundance: under these conditions, an unleashed Cyrano-driven TDMD activity acting on miR-7 might reach a limit in miR-7 degradation rate which cannot be further enhanced by an additional TDMD-competent target such as lin*Cdr1as* (Figure 3). In the presence of *Cdr1as*, the system would be set to intermediate miR-7 degradation rates which could be further enhanced by other TDMD-competent RNAs such as lin*Cdr1as* (see model in Appendix Figure S1). Notably, a similar protection phenomenon has been observed in a prostate cancer cell line, where knockdown of circ*CSNK1G3* bearing TDMD-like binding sites for miR-181b/d decreased their abundance, while circ*CSNK1G3* overexpression increased it (Chen *et al*, 2019) (Figure S2F).

The molecular basis explaining the functional differences between circRNAs and their cognate linear transcripts in triggering TDMD, might obey to the structural properties affected by the circular-linear topology. Based on a previous report, whereas circRNAs inhibit PKR-mediated innate immune responses, their cognate linear counterpart transcripts cannot. The explanation behind this phenomenon seems to be the inherent ability of circRNAs to fold into more stable short local secondary structures compared to their linear counterpart transcripts. This in turn seems to lead to a more stable interaction between circRNAs and PKR (Liu *et al*, 2019). Based on similar principles –but with an opposite outcome– the greater tendency of circRNAs to form secondary structures could confer them an extra rigidity that could ultimately limit their capacity to drive TDMD. This seems in agreement with previous reports showing that an extended miRNA:target basepairing *per se* is not enough to trigger TDMD:

miRNA binding must also occur within a conformationally flexible region of the target for TDMD to be active (Pawlica *et al*, 2016; Li *et al*, 2021; Fuchs Wightman *et al*, 2018). In line with this idea, two in-depth studies have contributed to our understanding of TDMD by pinpointing the ubiquitin ligase ZSWIM8 as a mediator of the mechanism (Shi *et al*, 2020; Han *et al*, 2020). These findings showed that the binding of TDMD-competent target RNAs drives a conformation change on AGO proteins (loaded with specific miRNAs) that leads to their poly-ubiquitination and degradation, leaving the specific miRNAs unprotected and susceptible to degradation by general nucleases. The extra rigidity of circRNAs could preclude the conformational change of AGO, thus bypassing TDMD while remaining bound to the RISC complex. A recent report might be consistent with this view by showing differences between the thermodynamic properties of linear and circular RNA in binding to complementary short RNAs, favouring a model where circRNAs might bind to miRNAs more efficiently than their cognate linear RNAs (Petkovic *et al*, 2021).

An alternative explanation could relate to the differential ability of distinct RNA species in recruiting TDMD machinery factors such as ZSWIM8. In that sense, several characteristics of circRNAs could be critical, such as their lack of capping and poly-A tails. However, the latter seems dispensable for TDMD based on the fact that HSUR-1, which lacks a poly-A tail, effectively drives TDMD on miR-27 (Cazalla *et al*, 2010; Pawlica *et al*, 2016). Additionally, specific sequence elements within transcripts are required for TDMD. For instance, both the miR-7 and miR-17 binding sites that exist within known TDMD-inducing targets (Cyrano and HCMV's UL144-145 respectively), depend on sequences that are located outside of the miRNA site *per se* for efficiently triggering of TDMD (Lee *et al*, 2013; Kleaveland *et al*, 2018; Han *et al*, 2020). Such sequences might be absent or simply occluded within the more highly structured circRNAs, possibly explaining their observed inability to drive TDMD.

Interactions between miRNAs and competing-endogenous RNAs (ceRNAs) have received a broad attention in the recent years as they might represent a mechanism of miRNA inhibition (Tay *et al*, 2014). However, due to stoichiometry considerations, the likelihood that individual ceRNAs titrate the total amount of miRNA available for target repression seems limited (Denzler *et al*, 2014; Jens & Rajewsky, 2015; Bosson *et al*, 2014; Pinzón *et al*, 2017; Denzler *et al*, 2016). Instead, models where multiple ceRNAs regulate single miRNAs have been favoured (Ameres & Zamore, 2013; Dodbele *et al*, 2021). The case of *Cdr1as*-miR-7 pair might represent an outstanding example functioning in an analogous way: *Cdr1as* is

406 a highly expressed circRNA with > 60 evolutionarily conserved miR-7 binding sites based on previous
407 reports (Memczak *et al*, 2013; Hansen *et al*, 2013) (67 predicted sites for miR-7 in humans based on the
408 STARBASE/ENCORI database), significantly exceeding the average number of sites annotated for
409 circRNAs (based on Starbase/ENCORI database, see Dataset EV2). On the other hand, while *Cdr1as* is
410 highly expressed in human, rat and mouse brain, miR-7 tends to display medium to low expression. Our
411 results favour a model where the concerted interaction of multiple circRNAs with individual miRNAs
412 seems the most likely and relevant scenario in regulating miRNA stability. Interestingly, among the
413 miRNAs that are upregulated upon ZSWIM8 knockdown in mouse induced neurons (Shi *et al*, 2020), two
414 belong to the most highly "sponged" miRNAs according to our analysis (miR-7 and also miR-409-3p),
415 suggesting that such type of regulation might be acting in neuron differentiation and possibly in
416 pathophysiological conditions (Figure EV4B).

417 An increasing number of TDMD natural examples have arisen in the past few years, including both
418 endogenous and viral transcripts (Ameres *et al*, 2010; Cazalla *et al*, 2010; Bitetti *et al*, 2018; Ghini *et al*,
419 2018; Li *et al*, 2021; Simeone *et al*, 2022; Kingston *et al*, 2022). Furthermore, the discovery that TDMD is
420 more widespread than initially thought suggests that more examples will be discovered (Shi *et al*, 2020;
421 Han *et al*, 2020). In this scenario, circRNAs' capacity to evade such regulation could confer them an
422 advantage in regulating miRNA stability even (or especially) when involving highly complementary
423 pairing architectures that would otherwise drive TDMD in the context of linear RNAs. Our findings
424 suggesting that the most highly "sponged" miRNAs seem to engage in TDMD-like interactions with
425 circRNAs more frequently than the least "sponged" miRNAs seems in line with this idea. Although we
426 ignore the extent to which circularization may affect the thermodynamic and/or kinetic properties of
427 miRNA-target pairing, we speculate that, by avoiding TDMD, sites with TDMD-like architectures within
428 circRNAs might provide an enhanced stability and/or decreased dissociation rate relative to sites with
429 canonical architectures present within the more abundant linear transcripts. Accordingly, by binding
430 and sequestering miRNAs through TDMD-like architectures, certain combinations of circRNAs might
431 stabilize specific miRNAs, rendering them unavailable for TDMD even when expressed at an overall sub-
432 stoichiometric level relative to the whole set of linear targets present in the cell. This type of regulation
433 would in turn be compatible with a potential reversibility of circRNA's inhibitory function on miRNAs.

A complex and yet unresolved aspect of the role of circRNAs in regulating miRNAs relates to our inability to predict their outcome on canonical miRNA silencing activity. In this sense, depending on factors such as the relative binding site architectures and the relative stoichiometries of the molecules involved, different outcomes may be expected. For instance, miRNA stabilization by circRNAs could lead to greater average target repression due to increased abundance of the cognate miRNAs. This is consistent with the effect that we observe in primary neurons upon *Cdr1as* KD (Appendix Figure S2B) and with previously published analysis in mouse cortex upon *CDR1as* knockout (Piwecka *et al*, 2017), where miR-7 predicted targets are significantly upregulated upon *CDR1as* knockout. However, miRNA stabilization by circRNAs could alternatively be accompanied by an overall tight blockade of miRNA silencing activity, leading to the opposite outcome in such contexts. Accordingly, our reanalysis of the data from a prostate cancer model (Chen *et al*, 2019) shows that a decrease of miR-181b/d upon circ*CSNK1G3* knockdown (analogous the case of miR-7 and *Cdr1as*) leads to an overall downregulation of miR-181b/d predicted targets. Our side-by-side reanalysis of both datasets from these reports suggests an overall opposite effect of specific miRNA stabilization by circRNAs on target silencing in these different cellular contexts (Appendix Figures S2B-E). Based on this, a direct correlation between the eventual stabilization of miRNAs by circRNAs and their ensuing downstream effect on miRNA canonical silencing cannot be currently established, highlighting the need of further dissecting the role of circRNAs on miRNA target repression. Eventually, more in-depth knowledge of the players involved, their relative stoichiometries and dynamics will help us understand the emergent properties arising from different systems and the full potential and adaptive value of circRNAs in miRNA regulation.

Limitations of the study

In this study we have generated a vector capable of expressing a circRNA with reduced levels of the linear "leak" RNA that is otherwise inevitably produced from these kinds of constructs. As shown in this work, although the principle works in our hands, the net circRNA-to-linear RNA relative expression yield that we obtain is still suboptimal. Bearing this limitation in mind, our data support the notion that the circRNA levels that we achieve are enough to prevent TDMD, either by not contributing to any additional TDMD effect and/or by antagonizing the TDMD driven by its co-expressed linear counterpart.

We are aware that effectively expressing circRNAs from artificial vectors is a general debate in the field, and we hope that our efforts to generate an improved system for circRNA expression might contribute to the development of even better strategies in the future.

It is important to stress the idea that additional properties of different circRNAs might determine their ability to bypass TDMD, including but not limited to circRNA modifications (RNA methylation, etc) and specific secondary structures, none of which have been systematically addressed in our work. More studies will be required to determine whether the avoidance of TDMD by circRNAs in particular and the ensuing miRNA stabilization in general, is a widespread phenomenon.

Furthermore, we have shown that a group of miRNAs sharing high "availability" of sites on circRNAs relative to their own abundance (defined above as "sponging suffered" coefficient) is preferably upregulated across a neuron-like differentiation. It is worth emphasizing that this correlation does not imply causality and that functional experiments will be needed in the future in order to validate this possibility. Finally, the enrichment of TDMD-like sites that we report in this study is based solely on predicted –though not experimentally validated– sites using the scanMiR bioinformatic tool (Soutschek *et al*, 2022).

Materials and methods

Plasmid construction

Unless otherwise specified, the lentiviral vectors are based on pRRLSIN.cPPT.SYN.WPRE (de la Mata *et al*, 2015).

Linear *Cdr1as* (lin*Cdr1as*) was amplified by PCR from rat genomic DNA (see primers at Table EV1). Following gel purification (QIAquick Gel Extraction Kit), and cloning into pCR II-Blunt-TOPO (ThermoFisher) it was then subcloned into pRRLSIN.cPPT.SYN.WPRE. The linear *Cdr1as* version lacking the sh*Cdr1as* target site –lin*Cdr1as*$^{671-}$ was generated by PCR amplification of a *Cdr1as* fragment lacking a 174-bp 3'-terminal segment that encompasses the miR-671 binding site, and re-cloning it into the original backbone's BamHI-SalI sites (Table EV1). The linear transcript used as a negative control consists of GFP expressed from pRRLSIN.cPPT.PGK-GFP.WPRE (Addgene plasmid 12252).

The pri-miR-132 and pri-miR-124 expressing constructs were made by amplifying the pri-miRNA fragments (Table EV1) from miRNASelectTM pEGP-mmu-mirna expression vectors (Cell Biolabs) and subsequently cloning them into the BamHI-BsrGI sites of pRRLSIN.cPPT.SYN.WPRE.

The shRNAmiR (sh*Cdr1as*) is an engineered version miR-671 –previously described as a natural *Cdr1as* regulator (Piwecka *et al*, 2017; Kleaveland *et al*, 2018)– designed to be fully complementary to the circRNA and maximizing its slicing capacity (Figure EV3A). The sh*Cdr1as* lentiviral vector was constructed by replacing the pri-miRNA fragments from the previously described vectors using BamHI-NheI (Table EV1), and inserting a synthetic DNA (gBlock gene fragment, IDT) by Gibson Assembly (Gibson *et al*, 2009).

CircRNA-expressing constructs were constructed inserting gBlocks (Integrated DNA Technologies) encompassing the ZKSCAN1 upstream and downstream introns (Liang & Wilusz, 2014) flanking mCherry and bulged or seed-mutant miR-132 sites (de la Mata *et al*, 2015) downstream of a Tetracyclin-inducible promoter (TREp, see Figure 1A and Table EV1). Perfect or seed-mutant sites for miR-124 were subsequently inserted downstream or the circularizable region (Figure EV1A). Linear TDMD inducers expressing mCherry upstream of bulged or seed-mutant miR-132 sites were previously described (de la Mata *et al*, 2015).

The lentiviral vector driving expression of FLAG/HA-AGO2 (human) from the Syn promoter (pLV-FLAG-HA_AGO2) was generated by amplifying FLAG/HA-AGO2 from pIRESneo-FLAG/HA AGO2 (Addgene plasmid 10822).

The construct for CRISPR/Cas9 genome editing of *Cdr1as* splicing sites is based on lentiCRISPRv2 (Addgene plasmid 52961), following the Zhang Lab protocol (Sanjana *et al*, 2014; Shalem *et al*, 2014) (Primers in Table EV1).

HEK293T culture and transient transfection

HEK293T cells were available in our institute. Cells were tested for mycoplasma contamination and only clean stocks were further used for our experiments. Cells were grown in DMEM-F12 (Gibco) supplemented with 10% (v/v) FCS and 25 U/mL Penicillin-Streptomycin (Gibco) and were plated for transfection at 100,000 cells/well on 24-well plates. One day after plating, cells were transfected using the PEI method as previously described (de la Mata *et al*, 2015).

Lentivirus production and transduction

Recombinant lentiviral particles were produced in HEK293T cell line. Cells were co-transfected using the PEI method with the lentiviral expression vector and two 2nd generation lentiviral packaging vectors: pMD2.G expressing the VSV-G envelope gene (Addgene plasmid 12259) and pCMVR8.74 expressing the gag/pol genes (Addgene plasmid 22036). The supernatants containing the viral particles were collected 48–72 h after transfection, concentrated using centrifugal filter units (Amicon Ultra-15, molecular weight cutoff 100 kDa, Millipore Cat. #UFC910024) as further checked as previously described (de la Mata *et al*, 2015).

Animals used in this study

All animal tissues used in this study were obtained under experiment protocol no. No.2020-04-DR with the approval from the Comisión Institucional para el Cuidado y Uso de los Animales de Laboratorio (CICUAL) at the Instituto de Investigación en Biomedicina de Buenos Aires (IBioBA) – CONICET – Partner Institute of the Max Planck Society.

Neuronal cultures and lentiviral transduction

Cortical and hippocampal neurons were dissected from embryonic day 16.5 and 18.5 (E16.5 and E18.5) respectively CD1 embryos of mixed sex. Culture preparation was performed as previously described (Giusti *et al*, 2014; Vogl *et al*, 2015). Briefly, cortex from CD1 mouse embryos were dissected and a neuronal suspension was prepared through Trypsin digestion and mechanical disruption of the tissue. Neurons were plated in 24 multi-well plates at a density of 80cells/mm2 (150.000 cells per well) and maintained in Neurobasal-A media (ThermoFisher) with 2% B27 and 0.5 mMGlutaMAX-I (ThermoFisher) at 37 °C and 5% CO2. CD1 mice for neuronal cultures were provided by our Specific Pathogen Free Animal Facility.

The euthanasia of the animals to generate primary neuronal cultures was performed under experiment protocol no. 2020-04-DR which was evaluated by the Institutional Animal Care and Use Committee of the IBioBA-CONICET according to the Principles for Biomedical Research involving

546 animals of the Council for International Organizations for Medical Sciences and provisions stated in the
547 Guide for the Care and Use of Laboratory Animals.

548 Neurons were transduced 4-7 days after plating (DIV4-7) with lentiviral constructs: lin*Cdr1as*$^{671\text{-}}$,
549 sh*Cdr1as*, the linear control or a combination of these, appropriately described in Results and Figures.
550 The vectors driving each of the circRNA-expressing constructs were transduced in combination with a
551 lentiviral construct expressing the tetracycline-controlled transactivator protein (LV-Syn-tTA). RNA was
552 extracted at DIV11 as indicated below.

553

554 **FLAG/HA-AGO2 transfection and immunoprecipitation (AGO2 RIP)**

555 The FLAG/HA-AGO2 expressing plasmid was transfected into HEK293T cells as described above.
556 Immunoprecipitation of FLAG/HA-AGO2 was performed with Anti-FLAG M2 Magnetic Beads (Sigma.
557 Cat # M8823). Beads were washed twice with TBS buffer (50 mM Tris HCl, 150 mM NaCl, pH 7.4). For each
558 immunoprecipitation (IP), one 6-cm plate with 50% confluency was used. Cells were washed once with
559 cold PBS and lyzed in 500 µl of lysis buffer [50 mM Tris–HCl pH 7.5, 150mM NaCl, 1% (v/v) TRITON X-100,
560 1 mM EDTA, containing protease inhibitors (cOmplete, EDTA-free Protease Inhibitor Cocktail, Roche)
561 and RNase inhibitor (Invitrogen)]. The lysates were incubated 30 minutes on ice, cleared by
562 centrifugation at 16,000 g for 10 minutes at 4 degrees and mixed with the washed beads. After 2 hours
563 of rotation at 4 degrees, the beads were washed three times with TBS buffer. As a control for the IPs,
564 non-transfected HEK293T cells were used. FLAG/HA-AGO2 expression and immunoprecipitation
565 efficiency were determined by Western blot using anti-HA antibody (clone 3F10, Roche). RNA was
566 extracted by adding Trizol reagent (Invitrogen) directly on the beads.

567

568 **Subcellular fractionation**

569 Briefly, the circRNA-expressing construct and the linear control were transfected into HEK293T cells
570 as described above, in 6-well plates at 50% confluency. After 48 hours, cells were harvested using 500
571 µl of PBS, transferred to a microcentrifuge tube and centrifuged at 500 g for 5 minutes. The supernatant
572 was discarded, and the pellet resuspended in 350 µl of PBS plus 0.1% NP-40 (IGEPAL). 150 µl were
573 separated and called TOTAL fraction. The remaining volume was centrifuged for 10 seconds at 10,000
574 rpm. 150 µl of the supernatant were separated and called CYTOPLASM fraction. The pellet was

resuspended in 150 ⌧l of PBS plus 0.1% NP-40 (IGEPAL) and centrifuged again at 10,000 rpm. The supernatant was discarded, and the pellet resuspended in 150 ⌧l of PBS plus 0.1% NP-40 (IGEPAL). This was called the NUCLEAR fraction.

Out of the 150 ⌧l of each fraction, 75 ⌧l were used for Western Blotting and 75 ⌧l for RNA extraction followed by reverse transcription and quantitative polymerase chain reaction (RT-qPCR).

RNA extraction

Total RNA extractions were made using Trizol reagent (Invitrogen) following the manufacturer's instructions.

RT-qPCR quantification

MiRNA and *U6* expression levels were determined by using Taqman® microRNA Assays (Applied Biosystems) following the manufacturer's instructions or using SYBR Green and step-loop RT-qPCR (see Table EV3 for oligo design). MicroRNA levels were normalized to *U6* RNA levels. Standard curves for the analysed miRNAs and *U6* RNA were performed with serial dilutions of selected cDNAs, allowing calculation of relative abundances. For quantification of target mRNAs, the artificial circRNA and *Cdr1as*, total RNA was treated with RNase-free Dnase I (DNA-freeTM Kit, Ambion) and reverse transcribed using random hexamers and SuperScriptTM II Reverse Transcriptase (Invitrogen) or MMLV-RT (Sigma), following the manufacturer's instructions. The abundance of target mRNAs, artificial circRNA and *Cdr1as* were determined by SYBR green qPCR using a custom-made qPCR mix (Table EV2) and specific primers (detailed at Table EV3). Alternatively, INBIO highway qPCR SYBR green mix was used (Ref M130). Standard curves for the analysed amplicons were performed with serial dilutions of selected cDNAs, allowing calculation of relative abundances.

Northern blot analysis

Northern blot analysis was performed according to standard procedures (Roditi *et al*, 1987). A total amount of 10 ⌧g of RNA was loaded in each lane. The radioactively labelled probe, corresponding to the mCherry CDS fragment, was prepared using the Megaprime DNA labelling kit (Amersham Biosciences) according to manufacturer's instructions. The 18S RNA from the agarose gel run was used

as loading control. Blots were hybridized at 65° and washed in 0.2× SSC/0.1% SDS. The blots were exposed to Phosphorimager screens and scanned with Typhoon FLA 7000 (GE Healthcare Life Sciences). The relative intensities of the bands were measured by densitometry using ImageJ.

Western blot analysis

Protein samples were separated on 12% SDS-polyacrylamide gels and transferred to PVDF membranes. Membranes were incubated with primary antibodies: anti-HA 3F10 (Rat, 1:2500), anti-Tubulin (polyclonal rabbit anti β Tubulin H-235 from Santa Cruz Biotechnology, 1:2500) and Histone-3 (polyclonal rabbit anti H3 H-0164 from Merk, 1:2500). After washing, membranes were incubated with IRDye® 800CW (LI- COR Biosciences) secondary antibodies. Bound antibody was detected an Odyssey imaging system (LI-COR Biosciences).

Statistical analysis

R programming language was used to process information, visualize and design graphs, and perform statistical tests. Data was normalized and scaled across experiments using Unit Length Normalization. Bar, line, scatter, dot and boxplots were designed using the ggplot2 (Wickham, 2016) and ggpubr packages. Statistical tests were done using base R and/or ggpubr (and its complement rstatix) (https://rpkgs.datanovia.com/ggpubr/index.html). For experiments where two conditions were compared, we performed unpaired t-tests, and for those where multiple comparisons were made, we used the Bonferroni correction (ns: $p > 0.05$, *: $p <= 0.05$, **: $p <= 0.01$, ***: $p <= 0.001$, ****: $p <= 0.0001$). For comparisons involving multiple groups we used either ANOVA followed by Tukey multiple comparisons, Generalized Linear Models (GLM) with emmeans (https://github.com/rvlenth/emmeans), or Wilcoxon rank sum test p-values (corrected with the Hochberg method for multiple comparisons) as indicated in the text. When comparing several miR-7 targets across conditions, we performed a two-way ANOVA followed by Tukey multiple comparisons, showing the adjusted p-value.

Bioinformatic analysis of circRNA-miRNA interactions

Two publicly available datasets produced by the Chen Lab were combined to generate a comprehensive analysis taking into account miRNA, circRNA and mRNA expression during

differentiation of H9 (hESC) cells to H9 forebrain neurons. From GEO Accession GSE73325 (Zhang *et al*, 2016) we obtained data for circRNA and mRNA expression. From GEO Accessions GSE56152 and GSE63709 (Chen *et al*, 2015) we obtained data for microRNA expression. Noteworthy, although the same procedure for differentiation was followed (Zhang *et al*, 2016; Chen *et al*, 2015), sequencing was done on different days (D26 and D35, respectively). We realize this is suboptimal, nevertheless we proceeded with the analysis considering this the best data available to approach our questions.

Data of the interactions between circRNAs and miRNAs was retrieved from Starbase/ENCORI v3 database (http://starbase.sysu.edu.cn; (Yang *et al*, 2011; Li *et al*, 2014)). This particular source was selected because it combines site prediction by several programs with experimental validation (e.g., by CLIP). The main parameters chosen for downloading through their API were: assembly = hg19, geneType= circRNA & miRNA, clipExpNum=1, program= all, programNum= 2, target= all and cellType= all.

A condensed spreadsheet summarizing all the previously mentioned data can be found at Dataset EV3.

The analysis was done in R, briefly:

- The expression tables were loaded and merged using the Tidyverse package (Wickham *et al*, 2019) and/or the readxl package (Wickham & Bryan, 2022), while the circRNA-miRNA interactions table was joined using the Fuzzyjoin package (https://CRAN.R-project.org/package=fuzzyjoin) to consider genomic locations of both the circRNAs and the miRNA sites.
- Log_2 fold changes across differentiation were calculated for each type of RNA.

Analysis from a miRNA perspective:

- An absolute number of validated miRNA-specific sites on every circRNA (when present) was calculated.
- A relative number of effective miRNA-specific sites was calculated by weighing the above number (i.e. the absolute number of miRNA-specific sites on every circRNA) to the number of backspliced junction reads as an estimate of the contribution of each circRNA.
- A total number of effective sites was calculated per miRNA (referred to as "miRNA-specific effective sites" later on) by summing all the effective miRNA-specific sites among all circRNAs,.

- A coefficient of "sponging suffered" by each miRNA was defined by dividing the above number ("miRNA-specific effective sites") by the miRNA abundance pre-differentiation. To simplify the analysis, we separated miRNAs in quartiles of increasing sponging suffered coefficients and performed the downstream analysis based on them.

Analysis from a circRNA perspective:

- The sum of all (i.e. pooling all miRNAs) absolute numbers of validated miRNA sites on each circRNA (when present) was calculated.
- The "sponging capacity" index for each circRNA was calculated by multiplying the above number to the number of junction reads pre-differentiation.

All graphs were programmed and illustrated using the packages ggplot2 (Wickham, 2016), ggrepel (https://CRAN.R-project.org/package=ggrepel) and/or viridis (https://CRAN.R-project.org/package=viridis). The network diagram (Figure EV4A) was done using IGraph package (https://igraph.org/r/). Statistical analysis of the boxplots was done and added to the graphs using ggpubr (https://rpkgs.datanovia.com/ggpubr/index.html).

For pri-miRNA analysis we used the Galaxy platform (The Galaxy platform for accessible, reproducible and collaborative biomedical analyses: 2022 update., 2022). Briefly, raw reads extracted from GSE73325 were trimmed using Trim Galore! (https://github.com/FelixKrueger/TrimGalore) and mapped to the human reference genome (hg38) with the RNA-STAR aligner (Dobin *et al*, 2013). Pri-miR counts were obtained from the mapped BAM files using featureCounts (Liao *et al*, 2014) and the annotation file (has.gff3) retrieved from miRBase (Kozomara *et al*, 2019).

Bioinformatic prediction of TDMD-like sites on circRNAs

To predict TDMD-like sites on circRNAs, we used the scanMiR package (Soutschek *et al*, 2022). Briefly, all reported human circRNA sequences were retrieved from circBase (Glažar *et al*, 2014) and used as an input for the *findSeedMatches* function from scanMiR to predict TDMD-like sites for every miRNA present. The data was filtered to keep only those sites on circRNAs that had at least one junction read in the neuron-like differentiation data (see above). Finally, we calculated the proportion of miRNAs with

predicted TDMD-like sites (computed as those with at least one TDMD-like site on circRNAs/linear RNAs) within each of the quartiles of increasing "sponging suffered" coefficients. Fisher's Exact tests between each quartile and the least "sponged" quartile ("- sponged") were performed to assess enrichment. The ggpie and rstatix packages were used to generate the pie charts and the ggpubr package to do the violin plot and t-tests.

Bioinformatic analysis of miR-7 and miR-181b/d targets

Targets for miR-7 were retrieved from TargetScan 7.1 mouse (Agarwal *et al*, 2015) while the ones for miR-181b/d from TargetScan 7.2 human (Agarwal *et al*, 2015). Raw RNA-seq counts were downloaded for *Cdr1as* KO data (Piwecka *et al*, 2017) and circCSNK1G3 KD (Chen *et al*, 2019), accessions GSE93130 and GSE113124, respectively. A differential expression analysis was performed using the DESeq2 package (Love *et al*, 2014). Graphs were made using the results of the analysis and the packages mentioned above.

Data availability

This study did not produce novel next generation sequencing datasets. Scripts and functions used to produce the results and plots shown in this paper can be found at: https://github.com/mmataLab/ciR-miR-stability

Acknowledgements

We thank Isabel Roditi for providing materials and discussing experiments, Helge Grosshans**,** Alberto R. Kornblihtt, Jeremy Wilusz and Javier Cáceres for a critical reading of the manuscript, Pierre-Luc Germain for a critical reading and general discussion of the manuscript, Valeria Buggiano for technical assistance and Luciana Giono for creating figure illustrations. M.d.l.M. is funded by grants from Agencia Nacional de Promocion Cientifica y Tecnológica (ANPCyT) of Argentina (PICT- 2016-0499 and PICT-2018-0478_PRH 2016-0002). D.R. acknowledges the support of the Volkswagen, Stiftung, the Max Planck Society, the Fondo para la Convergencia Estructural de Mercosur (COF 03/11), the Agencia Nacional de

718 Promoción Científica y Tecnológica (ANPCyT) of Argentina (PICT- 2019-0499 and PICT-PRH 2014-3782)
719 and the Ministerio de Ciencia, Tecnología e Innovación Productiva of Argentina (MinCyT-BMBF
720 AL15/10). J.P.F. is funded by grants from Ministerio de Ciencia, Tecnología e Innovación Productiva of
721 Argentina (MINCyT) (BMBF/MINCYT MIGRAMIRNA AI/17/05), Agencia Nacional de Promocion Cientifica
722 y Tecnologica (ANPCyT) of Argentina (PICT-2017-2401, PCE-GSK-2017-0052), Glaxo-SmithKline (PCE-
723 GSK-2017-0052) and Fundación Progreso de la Medicina (GF N03/2017).

724

725 Author contributions

726 D.R. and M.d.l.M. conceived the project and designed and interpreted the experiments. F.F.W. and
727 J.L. designed, performed and interpreted most of the experiments. F.F.W. conceived, performed and
728 interpreted most of the computational analysis. M.d.l.M. conceived, performed and interpreted some of
729 the computational analysis. G.S. and M.S. contributed with the use of the scanMiR package to obtain
730 the TDMD-like site enrichment results and discussed strategies for data analysis. J.L. and S.G. handled
731 animals and prepared the neuron primary cultures. L.B. performed the subcellular fractionation
732 experiments. B.P. performed the Northern blot analysis. P.G. performed the subcloning of some of the
733 constructs used in the study. J.P.F. designed some of the experiments and discussed experimental
734 strategies. D.R. and M.d.l.M. co-supervised the whole project. The manuscript was written by F.F.W., D.R.
735 and M.d.l.M.

736

737 Conflict of interest

738 The authors declare that they have no conflict of interest.

References

Agarwal V, Bell GW, Nam JW & Bartel DP (2015) Predicting effective microRNA target sites in mammalian mRNAs. *eLife* 4: 1–38

Ameres SL, Horwich MD, Hung J-H, Xu J, Ghildiyal M, Weng Z & Zamore PD (2010) Target RNA-directed trimming and tailing of small silencing RNAs. *Science* 328: 1534–1539

Ameres SL & Zamore PD (2013) Diversifying microRNA sequence and function. *Nat Rev Mol Cell Biol* 14: 475–488

Bartel DP (2018) Metazoan MicroRNAs. *Cell* 173: 20–51

Bitetti A, Mallory AC, Golini E, Carrieri C, Carreño Gutiérrez H, Perlas E, Pérez-Rico YA, Tocchini-Valentini GP, Enright AJ, Norton WHJ, *et al* (2018) MicroRNA degradation by a conserved target RNA regulates animal behavior. *Nat Struct Mol Biol* 25: 244–251

Bosson AD, Zamudio JR & Sharp PA (2014) Endogenous miRNA and target concentrations determine susceptibility to potential ceRNA competition. *Mol Cell* 56: 347–359

Brown BD, Gentner B, Cantore A, Colleoni S, Amendola M, Zingale A, Baccarini A, Lazzari G, Galli C & Naldini L (2007) Endogenous microRNA can be broadly exploited to regulate transgene expression according to tissue, lineage and differentiation state. *Nat Biotechnol* 25: 1457–1467

Cazalla D, Yario T & Steitz JA (2010) Down-regulation of a host microRNA by a Herpesvirus saimiri noncoding RNA. *Science* 328: 1563–1566

Chen L-L (2020) The expanding regulatory mechanisms and cellular functions of circular RNAs. *Nat Rev Mol Cell Biol* 21: 475–490

Chen S, Huang V, Xu X, Livingstone J, Soares F, Jeon J, Zeng Y, Hua JT, Petricca J, Guo H, *et al* (2019) Widespread and Functional RNA Circularization in Localized Prostate Cancer. *Cell* 176: 831-843.e22

Chen T, Xiang J-F, Zhu S, Chen S, Yin Q-F, Zhang X-O, Zhang J, Feng H, Dong R, Li X-J, *et al* (2015) ADAR1 is required for differentiation and neural induction by regulating microRNA processing in a catalytically independent manner. *Cell Res* 25: 459–476

Conn SJ, Pillman KA, Toubia J, Conn VM, Salmanidis M, Phillips CA, Roslan S, Schreiber AW, Gregory PA & Goodall GJ (2015) The RNA binding protein quaking regulates formation of circRNAs. *Cell* 160: 1125–1134

768 de la Mata M, Gaidatzis D, Vitanescu M, Stadler MB, Wentzel C, Scheiffele P, Filipowicz W & Großhans H
769 (2015) Potent degradation of neuronal miRNAs induced by highly complementary targets.
770 *EMBO Rep* 16: 500–511
771 Denzler R, Agarwal V, Stefano J, Bartel DP & Stoffel M (2014) Assessing the ceRNA hypothesis with
772 quantitative measurements of miRNA and target abundance. *Mol Cell* 54: 766–776
773 Denzler R, McGeary SE, Title AC, Agarwal V, Bartel DP & Stoffel M (2016) Impact of MicroRNA Levels,
774 Target-Site Complementarity, and Cooperativity on Competing Endogenous RNA-Regulated
775 Gene Expression. *Mol Cell* 64: 565–579
776 Dobin A, Davis CA, Schlesinger F, Drenkow J, Zaleski C, Jha S, Batut P, Chaisson M & Gingeras TR (2013)
777 STAR: ultrafast universal RNA-seq aligner. *Bioinformatics* 29: 15–21
778 Dodbele S, Mutlu N & Wilusz JE (2021) Best practices to ensure robust investigation of circular RNAs:
779 pitfalls and tips. *EMBO Rep* 22: e52072
780 Fellmann C, Hoffmann T, Sridhar V, Hopfgartner B, Muhar M, Roth M, Lai DY, Barbosa IAM, Kwon JS, Guan
781 Y, *et al* (2013) An optimized microRNA backbone for effective single-copy RNAi. *Cell Rep* 5:
782 1704–1713
783 Fuchs Wightman F, Giono LE, Fededa JP & de la Mata M (2018) Target RNAs Strike Back on MicroRNAs.
784 *Front Genet* 9: 435
785 Gasparini S, Licursi V, Presutti C & Mannironi C (2020) The Secret Garden of Neuronal circRNAs. *Cells* 9:
786 1815
787 Ghini F, Rubolino C, Climent M, Simeone I, Marzi MJ & Nicassio F (2018) Endogenous transcripts control
788 miRNA levels and activity in mammalian cells by target-directed miRNA degradation. *Nat*
789 *Commun* 9: 3119
790 Gibson DG, Young L, Chuang R-Y, Venter JC, Hutchison CA 3rd & Smith HO (2009) Enzymatic assembly
791 of DNA molecules up to several hundred kilobases. *Nat Methods* 6: 343–345
792 Giusti SA, Vogl AM, Brockmann MM, Vercelli CA, Rein ML, Trümbach D, Wurst W, Cazalla D, Stein V,
793 Deussing JM, *et al* (2014) MicroRNA-9 controls dendritic development by targeting REST. *Elife*
794 3: e02755
795 Glažar P, Papavasileiou P & Rajewsky N (2014) circBase: a database for circular RNAs. *RNA* 20: 1666–1670

796 Guarnerio J, Zhang Y, Cheloni G, Panella R, Mae Katon J, Simpson M, Matsumoto A, Papa A, Loretelli C,
797 Petri A, *et al* (2019) Intragenic antagonistic roles of protein and circRNA in tumorigenesis. *Cell*
798 *Res* 29: 628–640
799 Guo JU, Agarwal V, Guo H & Bartel DP (2014) Expanded identification and characterization of
800 mammalian circular RNAs. *Genome Biol* 15: 409
801 Han J, LaVigne CA, Jones BT, Zhang H, Gillett F & Mendell JT (2020) A ubiquitin ligase mediates target-
802 directed microRNA decay independently of tailing and trimming. *Science* 370: eabc9546
803 Hanan M, Simchovitz A, Yayon N, Vaknine S, Cohen-Fultheim R, Karmon M, Madrer N, Rohrlich TM,
804 Maman M, Bennett ER, *et al* (2020) A Parkinson's disease CircRNAs Resource reveals a link
805 between circSLC8A1 and oxidative stress. *EMBO Mol Med* 12: e11942
806 Hansen TB, Jensen TI, Clausen BH, Bramsen JB, Finsen B, Damgaard CK & Kjems J (2013) Natural RNA
807 circles function as efficient microRNA sponges. *Nature* 495: 384–388
808 Hansen TB, Wiklund ED, Bramsen JB, Villadsen SB, Statham AL, Clark SJ & Kjems J (2011) miRNA-
809 dependent gene silencing involving Ago2-mediated cleavage of a circular antisense RNA.
810 *EMBO J* 30: 4414–4422
811 Jeck WR, Sorrentino JA, Wang K, Slevin MK, Burd CE, Liu J, Marzluff WF & Sharpless NE (2013) Circular
812 RNAs are abundant, conserved, and associated with ALU repeats. *RNA* 19: 141–157
813 Jens M & Rajewsky N (2015) Competition between target sites of regulators shapes post-transcriptional
814 gene regulation. *Nat Rev Genet* 16: 113–126
815 Jonas S & Izaurralde E (2015) Towards a molecular understanding of microRNA-mediated gene
816 silencing. *Nat Rev Genet* 16: 421–433
817 Kingston ER, Blodgett LW & Bartel DP (2022) Endogenous transcripts direct microRNA degradation in
818 Drosophila, and this targeted degradation is required for proper embryonic development. *Mol*
819 *Cell*: S1097-2765(22)00849–8
820 Kleaveland B, Shi CY, Stefano J & Bartel DP (2018) A Network of Noncoding Regulatory RNAs Acts in the
821 Mammalian Brain. *Cell* 174: 350-362.e17
822 Kozomara A, Birgaoanu M & Griffiths-Jones S (2019) miRBase: from microRNA sequences to function.
823 *Nucleic Acids Res* 47: D155–D162

824 Kramer MC, Liang D, Tatomer DC, Gold B, March ZM, Cherry S & Wilusz JE (2015) Combinatorial control
825 of Drosophila circular RNA expression by intronic repeats, hnRNPs, and SR proteins. *Genes Dev*
826 29: 2168–2182
827 Kristensen LS, Andersen MS, Stagsted LVW, Ebbesen KK, Hansen TB & Kjems J (2019) The biogenesis,
828 biology and characterization of circular RNAs. *Nat Rev Genet* 20: 675–691
829 Krol J, Busskamp V, Markiewicz I, Stadler MB, Ribi S, Richter J, Duebel J, Bicker S, Fehling HJJ, Schubeler
830 D, *et al* (2010) Characterizing light-regulated retinal microRNAs reveals rapid turnover as a
831 common property of neuronal microRNAs. *Cell* 141: 618–631
832 Lee S, Song J, Kim S, Kim J, Hong Y, Kim Y, Kim D, Baek D & Ahn K (2013) Selective degradation of host
833 MicroRNAs by an intergenic HCMV noncoding RNA accelerates virus production. *Cell Host*
834 *Microbe* 13: 678–690
835 Li J-H, Liu S, Zhou H, Qu L-H & Yang J-H (2014) starBase v2.0: decoding miRNA-ceRNA, miRNA-ncRNA
836 and protein-RNA interaction networks from large-scale CLIP-Seq data. *Nucleic Acids Res* 42:
837 D92-97
838 Li L, Sheng P, Li T, Fields CJ, Hiers NM, Wang Y, Li J, Guardia CM, Licht JD & Xie M (2021) Widespread
839 microRNA degradation elements in target mRNAs can assist the encoded proteins. *Genes Dev*
840 35: 1595–1609
841 Li X, Liu C-X, Xue W, Zhang Y, Jiang S, Yin Q-F, Wei J, Yao R-W, Yang L & Chen L-L (2017) Coordinated
842 circRNA Biogenesis and Function with NF90/NF110 in Viral Infection. *Mol Cell* 67: 214-227.e7
843 Liang D & Wilusz JE (2014) Short intronic repeat sequences facilitate circular RNA production. *Genes and*
844 *Development* 28: 2233–2247
845 Liao Y, Smyth GK & Shi W (2014) featureCounts: an efficient general purpose program for assigning
846 sequence reads to genomic features. *Bioinformatics* 30: 923–930
847 Litke JL & Jaffrey SR (2019) Highly efficient expression of circular RNA aptamers in cells using
848 autocatalytic transcripts. *Nat Biotechnol* 37: 667–675
849 Liu CX, Li X, Nan F, Jiang S, Gao X, Guo SK, Xue W, Cui Y, Dong K, Ding H, *et al* (2019) Structure and
850 Degradation of Circular RNAs Regulate PKR Activation in Innate Immunity. *Cell* 177: 865-
851 880.e21

852 Love MI, Huber W & Anders S (2014) Moderated estimation of fold change and dispersion for RNA-seq
853 data with DESeq2. *Genome Biol* 15: 550
854 Marcinowski L, Tanguy M, Krmpotic A, Rädle B, Lisnić VJ, Tuddenham L, Chane-Woon-Ming B, Ruzsics Z,
855 Erhard F, Benkartek C, *et al* (2012) Degradation of cellular mir-27 by a novel, highly abundant
856 viral transcript is important for efficient virus replication in vivo. *PLoS Pathog* 8: e1002510
857 Memczak S, Jens M, Elefsinioti A, Torti F, Krueger J, Rybak A, Maier L, Mackowiak SD, Gregersen LH,
858 Munschauer M, *et al* (2013) Circular RNAs are a large class of animal RNAs with regulatory
859 potency. *Nature* 495: 333–338
860 Pamudurti NR, Bartok O, Jens M, Ashwal-Fluss R, Stottmeister C, Ruhe L, Hanan M, Wyler E, Perez-
861 Hernandez D, Ramberger E, *et al* (2017) Translation of CircRNAs. *Mol Cell* 66: 9-21.e7
862 Pawlica P, Moss WN & Steitz JA (2016) Host miRNA degradation by Herpesvirus saimiri small nuclear
863 RNA requires an unstructured interacting region. *RNA* 22: 1181–1189
864 Petkovic S, Graff S, Feller N, Berghaus J, Ruppert V-P, Dülfer J & Sczakiel G (2021) Circular versus linear
865 RNA topology: different modes of RNA-RNA interactions in vitro and in human cells. *RNA Biol*
866 18: 674–683
867 Pinzón N, Li B, Martinez L, Sergeeva A, Presumey J, Apparailly F & Seitz H (2017) microRNA target
868 prediction programs predict many false positives. *Genome Res* 27: 234–245
869 Piwecka M, Glažar P, Hernandez-Miranda LR, Memczak S, Wolf SA, Rybak-Wolf A, Filipchyk A, Klironomos
870 F, Cerda Jara CA, Fenske P, *et al* (2017) Loss of a mammalian circular RNA locus causes miRNA
871 deregulation and affects brain function. *Science* 357: eaam8526
872 Roditi I, Carrington M & Turner M (1987) Expression of a polypeptide containing a dipeptide repeat is
873 confined to the insect stage of Trypanosoma brucei. *Nature* 325: 272–274
874 Rybak-Wolf A, Stottmeister C, Glažar P, Jens M, Pino N, Giusti S, Hanan M, Behm M, Bartok O, Ashwal-
875 Fluss R, *et al* (2015) Circular RNAs in the Mammalian Brain Are Highly Abundant, Conserved,
876 and Dynamically Expressed. *Mol Cell* 58: 870–885
877 Salzman J, Chen RE, Olsen MN, Wang PL & Brown PO (2013) Cell-type specific features of circular RNA
878 expression. *PLoS genetics* 9: e1003777
879 Sanjana NE, Shalem O & Zhang F (2014) Improved vectors and genome-wide libraries for CRISPR
880 screening. *Nat Methods* 11: 783–784

Shalem O, Sanjana NE, Hartenian E, Shi X, Scott DA, Mikkelson T, Heckl D, Ebert BL, Root DE, Doench JG, *et al* (2014) Genome-scale CRISPR-Cas9 knockout screening in human cells. *Science* 343: 84–87

Shi CY, Kingston ER, Kleaveland B, Lin DH, Stubna MW & Bartel DP (2020) The ZSWIM8 ubiquitin ligase mediates target-directed microRNA degradation. *Science* 370: eabc9359

Simeone I, Rubolino C, Noviello TMR, Farinello D, Cerulo L, Marzi MJ & Nicassio F (2022) Prediction and pan-cancer analysis of mammalian transcripts involved in target directed miRNA degradation. *Nucleic Acids Res* 50: 2019–2035

Soutschek M, Gross F, Schratt G & Germain P-L (2022) scanMiR: a biochemically-based toolkit for versatile and efficient microRNA target prediction. *Bioinformatics*: btac110

Tay Y, Rinn J & Pandolfi PP (2014) The multilayered complexity of ceRNA crosstalk and competition. *Nature* 505: 344–352

The Galaxy platform for accessible, reproducible and collaborative biomedical analyses: 2022 update. (2022) *Nucleic Acids Res* 50: W345-351

Vogl AM, Brockmann MM, Giusti SA, Maccarrone G, Vercelli CA, Bauder CA, Richter JS, Roselli F, Hafner A-S, Dedic N, *et al* (2015) Neddylation inhibition impairs spine development, destabilizes synapses and deteriorates cognition. *Nat Neurosci* 18: 239–251

Wickham H (2016) Data Analysis. In *ggplot2: Elegant Graphics for Data Analysis*, Wickham H (ed) pp 189–201. Cham: Springer International Publishing

Wickham H, Averick M, Bryan J, Chang W, McGowan LD, François R, Grolemund G, Hayes A, Henry L, Hester J, *et al* (2019) Welcome to the Tidyverse. *Journal of Open Source Software* 4: 1686

Wickham H & Bryan J (2022) readxl: Read Excel Files. *https://readxl.tidyverse.org, https://github.com/tidyverse/readxl*

Xiao M-S, Ai Y & Wilusz JE (2020) Biogenesis and Functions of Circular RNAs Come into Focus. *Trends Cell Biol* 30: 226–240

Yang J-H, Li J-H, Shao P, Zhou H, Chen Y-Q & Qu L-H (2011) starBase: a database for exploring microRNA-mRNA interaction maps from Argonaute CLIP-Seq and Degradome-Seq data. *Nucleic Acids Res* 39: D202-209

908 You X, Vlatkovic I, Babic A, Will T, Epstein I, Tushev G, Akbalik G, Wang M, Glock C, Quedenau C, *et al*
909 (2015) Neural circular RNAs are derived from synaptic genes and regulated by development
910 and plasticity. *Nat Neurosci* 18: 603–610
911 Zhang XO, Wang H Bin, Zhang Y, Lu X, Chen LL & Yang L (2014) Complementary sequence-mediated
912 exon circularization. *Cell* 159: 134–147
913 Zhang Y, Xue W, Li X, Zhang J, Chen S, Zhang J-L, Yang L & Chen L-L (2016) The Biogenesis of Nascent
914 Circular RNAs. *Cell Rep* 15: 611–624
915

Figure legends

Figure 1.

System to artificially express circRNAs reducing their overlapping, cognate linear RNA expression.

A. Top: Illustration of the linear RNA expressing construct used as a positive control for TDMD (TDMD inducer). Bottom: Illustration of the circRNA-expressing construct; depicted with coloured arrows are the sets of primers used to measure the different transcript variants (circular [1], Total Output-TO [2] and linear [3]).

B. Total output (TO), linear and circular RNA levels upon expression of the circRNA-expressing constructs from the tetracycline-inducible promoter (TREp) bearing perfectly matched or seed-mutant miR-124 sites for selective linear RNA degradation (see Figure EV1A). n = 5 culture wells (from 3 independent primary cultures) of cortical neurons for each condition; and n = 7 culture wells (from 4 independent primary cultures) of hippocampal neurons for each condition.

C. Total reporter output (left) and circRNA levels (right) upon expression of the circRNA-expressing construct or the linear RNA construct (TDMD inducer). The constructs were expressed from the tetracycline-inducible promoter (TREp) and the synapsin (Syn) promoter respectively in order to achieve similar total output levels for both constructs n = 9 culture wells (from 3 independent primary cultures) of cortical neurons for each condition; n = 9 culture wells (from 4 independent primary cultures) of hippocampal neurons for each condition. Missing points are failed culture wells/RT-qPCR reactions.

In (B–C), data are presented as mean ± SEM. Statistical significance was determined by unpaired Student's *t* tests (ns: p > 0.05, *: p <= 0.05, **: p <= 0.01, ***: p <= 0.001, ****: p <= 0.0001).

Figure 2.

Artificial circRNA-expressing constructs are unable to trigger TDMD.

A MiR-132 abundance upon transduction of the linear control (left) or the circRNA-expressing construct (right) carrying bulged (TDMD-compatible) or seed-mutant miR-132 sites. n = 9 culture wells (from 3 independent primary cultures) of cortical neurons for each condition; n = 9 culture

wells (from 4 independent primary cultures) of hippocampal neurons for each condition. Missing points are failed culture wells/RT-qPCR reactions.

B AGO2-Flag immunoprecipitation (RIP) followed by RT-qPCR in HEK293T cells. MiR-27a was used to normalize expression. Relative circRNA abundance was measured using circRNA-backspliced-junction specific divergent primers and normalized to miR-27a levels as an unrelated RISC-loaded miRNA not expected to be affected by the circRNA. Levels of non-specific *U6* background binding to Ago2 are shown. As an IP quality control, FLAG/HA-AGO2 input levels were shown to be similar across transfected conditions and efficiently pulled-down using anti-FLAG beads (Figure EV2B). Accordingly, miR-27, but not *U6* RNA, was efficiently co-immunoprecipitated, showing an even recovery of Ago-bound RNA across transfected conditions (Figure EV2C). n = 4 culture wells (from 2 experiments) of HEK293T cells for each condition.

C Subcellular fractionation showing total vs. cytoplasmic (left) and total vs. nuclear (right) fractions, followed by RT-qPCR of the circRNA and linear RNA isoforms, normalized by *GAPDH* (for cytoplasm) or *U6* (for nucleus). Fractionation efficiency was assessed via Western Blot and RT-qPCR (Figure EV2D-E). n = 4 culture wells (from 2 experiments) of HEK293T cells for each condition.

In (A–C), data are presented as mean ± SEM . Statistical significance was determined by unpaired Student's *t tests* (ns: p > 0.05, *: p <= 0.05, **: p <= 0.01, ***: p <= 0.001, ****: p <= 0.0001).

Figure 3.

The topology of *Cdr1as* determines the outcome of its effect on miR-7's stability.

A *Cdr1as* total output levels (linear plus circular) measured by RT-qPCR upon transduction of either a scrambled shRNA or sh*Cdr1as* alone, or sh*Cdr1as* rescued with a linear version of *Cdr1as* (lin*Cdr1as*) lacking the *shCdr1as* site, in cortical primary neurons. n = 6 culture wells (from 3 independent primary cultures) for control and cirCDR1as KD; n = 4 culture wells (from 2 independent primary cultures) for lin*Cdr1as* rescue.

B MiR-7 abundance measured by Taqman RT-qPCR in the same samples as in A. n = 6 culture wells (from 3 independent primary cultures) for control and cirCDR1as KD; n = 4 culture wells (from 2 independent primary cultures) for lin*Cdr1as* rescue.

C *Cdr1as* total output levels measured by RT-qPCR upon over-expression of linear *Cdr1as* (lin*Cdr1as*) in primary hippocampal neurons. Control corresponds to a non-related (GFP-expressing) linear transcript. n = 6 culture wells (from 2 independent primary cultures) for each condition.

D MiR-7 abundance measured by Taqman RT-qPCR in the same samples as in C. n = 6 culture wells (from 2 independent primary cultures) for each condition.

Data are presented as mean ± SEM. Statistical significance was determined by unpaired Student's *t tests* (ns: p > 0.05, *: p <= 0.05, **: p <= 0.01, ***: p <= 0.001, ****: p <= 0.0001).

Figure 4.

CircRNAs potentially stabilize dozens of microRNAs across neuron-like differentiation.

A Scatter plot of miRNA expression fold changes (log2) across differentiation of hESC H9 cells into forebrain (FB) neuron progenitor cells plotted against the number of effective sites, coloured by quartiles of increasing number of "effective" sites within circRNAs.

B Scatter plot of miRNA fold changes (log2) across differentiation plotted against miRNA "sponging suffered" coefficient score (log10) coloured by quartiles in a scatter plot. The predicted most highly "sponged" miRNAs show the highest fold changes across differentiation.

C Boxplot depicting the fold changes (log2) across differentiation of miRNA separated by quartiles of increasing "sponging suffered" coefficients.

D Scatter plots of miRNA fold changes (log2) plotted against pri-miRNA fold changes (log2) faceted by "sponging suffered" coefficient quartiles. Indicated are the slopes (b) and p-values for the interaction terms of each quartile's curve against the reference ("-sponged") quartile within a multiple regression model with interaction.

E Boxplot showing circRNA expression fold changes (log2) across differentiation separated by quartiles of increasing "sponging capacity " index.

The analysis includes 236 miRNAs. For panels C and E, GLM with emmeans statistics are shown between the least sponged and the remaining groups (ns: p > 0.05, *: p <= 0.05, **: p <= 0.01, ***: p <= 0.001, ****: p <= 0.0001).

Figure 5.

Predicted TDMD-like site architectures within circRNAs are more frequent for the most highly "sponged" miRNAs

A Pie charts showing the proportion of linear RNA- and circRNA-miRNA interactions involving at least one predicted TDMD-like site against miRNAs within quartiles of increasing "sponging suffered" coefficients. Shown are the p-values for the Fisher's Exact test between each quartile and the least sponged quartile ("- sponged").

B Violin plots depicting the number of predicted TDMD-like sites within circRNAs against miRNAs belonging to quartiles of increasing "sponging suffered" coefficients. GLM with emmeans statistics are shown between the least sponged and the other quartiles (ns: $p > 0.05$, *: $p <= 0.05$, **: $p <= 0.01$, ***: $p <= 0.001$, ****: $p <= 0.0001$).

Expanded View Figure Legends

Figure EV1.

CircRNA-expressing constructs and quality controls.

A Table summarizing the generated constructs.

B Northern blot analysis of RNase R treated or untreated samples from HEK293T cells expressing the indicated constructs. CircRNAs are resistant to RNase R digestion, confirming the circular topology of the artificial circRNA. All constructs were expressed from the tetracycline-inducible promoter (TREp). The asterisk (*) marks a putative mechanically linearized product of the corresponding circRNA.

C Quantification by different methods of the linear and circular isoforms from RNase R untreated samples of HEK293T cells (naturally lacking miR124) expressing the indicated constructs. Top panels: digital densitometry quantification of Northern blot bands by ImageJ. Bottom panels: RT-qPCR quantification using primers specific for the circular isoform or for both the linear and circular isoforms combined (Total output) as depicted in Figure 1A. In red, the mean is indicated. n = 2 culture wells (from 1 experiment) of HEK293T cells for each condition.

D RT-qPCR measurement of the circRNA-to-linear RNA ratio of RNase R treated vs. untreated samples in cortical neurons or HEK293T cells using divergent primers depicted in Figure 1. Values reflect relative rather than absolute ratios of the measured isoforms. n = 3 culture wells (from 1 primary

culture/experiment) of each cell type and for each condition.E Top: Agarose gel showing triplicates of the qPCR amplicons obtained with divergent primers against the backsplicing junction of the artificial circRNA, after retro-transcription with two different reverse transcriptases (MMLV-RT & Superscript II) in order to rule out artifacts due to template switching during cDNA synthesis. Bottom: Sanger sequencing of the amplicons shown above confirming backsplicing junction in HEK293 cells.

Figure EV2.

TDMD specificity, HA-FLAG/AGO2 RIP and cellular fractionation quality controls.

A RT-qPCR quantification of the indicated RNA species confirms specific degradation of miR-132 guide strand (miR-132-3p) and discards potential transcriptional effects. Levels of miR-132 passenger strand (miR-132-5p), primary transcript (pri-miR-132) and four unrelated miRNAs (miR-124-3p, miR-128-3p, miR-138-5p and miR-409-3p) were normalized to *U6*. n = 9 culture wells (from 3 independent primary cultures) of cortical neurons for each condition; n = 9 culture wells (from 4 independent primary cultures) of hippocampal neurons for each condition. Missing points are failed culture wells/RT-qPCR reactions.

B Representative anti-HA Western Blot from inputs or anti-FLAG IPs in non-transfected HEK-293T cells or cells co-transfected with HA-FLAG/AGO2 and the circRNA-expressing construct bearing bulged (WT) or seed-mutant (mut) miR-132 sites.

C *U6* and miR-27 levels were measured to verify the efficiency of HA-FLAG/AGO2 immunoprecipitation. n = 4 culture wells (from 2 experiments) of HEK293T cells for each condition.

D Representative Western Blot of HEK293T cells transfected with either the circRNA-expressing construct or the linear control RNA, following subcellular fractionation. β-Tubulin and Histone-3 were used as cytoplasm and nucleus markers, respectively.

E Boxplot depicting median values of *GAPDH*/*U6* ratio measured by RT-qPCR confirms proper subcellular fractionation of samples either transfected with the circRNA-expressing construct or the linear control. n = 4 culture wells (from 1 experiment) of HEK293T cells for each condition.

In (A, C), data are presented as mean ± SEM. Statistical significance was determined by unpaired Student's *t tests* (ns: p > 0.05, *: p <= 0.05, **: p <= 0.01, ***: p <= 0.001, ****: p <= 0.0001). In panel A, Bonferroni's correction for multiple testing was applied.

Figure EV3.

MicroRNA site illustrations, quality controls and primer design for *Cdr1as*.

A Scheme depicting the sequences of the miR-671 binding site within *Cdr1as*, miR-671 and the engineered sh*Cdr1as*. The latter is based on miR-671 with two nucleotide changes that make it fully complementary to the circRNA to maximize its slicing capacity.

B Three examples of potential TDMD-competent binding sites for miR-7 present in *Cdr1as*, aligned and illustrated using scanMiR.

C Expression levels of *Cdr1as* total output, circular *Cdr1as* and unrelated gene (*Actb*) upon over-expression of linear *Cdr1as* (lin*Cdr1as*). Levels were normalized to *Gapdh*. n = 6 culture wells (from 2 independent primary cultures) for each condition.

D Expression levels of miR-7 guide strand (miR-7-5p), passenger strands (miR-7a-1-3p and miR-7a-2-3p), primary RNA (pri-miR-7a-1) and two unrelated miRNAs (miR-9-5p and miR-132-3p). All miRNAs levels were normalized to *U6*, while the pri-miR level was normalized to *Gapdh*. n = 6 culture wells (from 2 independent primary cultures) for each condition.

E Illustration of the strategy designed to mutate *Cdr1as* splicing sites by CRISPR/Cas9.

F *Cdr1as* total output levels upon CRISPR/Cas9 editing of the *Cdr1as* splicing sites, measured by RT-qPCR in primary hippocampal neurons. Control corresponds to a transduced linear transcript (GFP-expressing). n = 3 culture wells (from 1 independent primary culture) for each condition.

G MiR-7 abundance measured by Taqman RT-qPCR in the same samples as in F. n = 3 culture wells (from 1 independent primary culture) for each condition.

H Illustration of the primer designs for measuring the different *Cdr1as* isoforms (detailed in Materials and Methods).

Data are presented as mean ± SEM. Statistical significance was determined by unpaired Student's *t tests* (ns: p > 0.05, *: p <= 0.05, **: p <= 0.01, ***: p <= 0.001, ****: p <= 0.0001). In panels C and D, Bonferroni's correction for multiple testing was applied. For the F and G panels, equal variance was assumed.

Figure EV4.

Illustrations of the predicted circRNA-miRNA networks and genomic features of the potentially involved circRNAs.

A Network diagram of biochemically supported interactions between circRNAs and miRNAs. Depicted are the interactions involving the seven most "sponging" circRNAs.

B Network diagram showing biochemically supported circRNA-miRNA interactions for miR-7 and two other miRNAs with similar "sponging" coefficient (miR-670-3p and miR-409-3p). For all three examples, the stoichiometries (i.e. ratios of circRNA-binding-site:miRNA) are similar, with CDR1as making the largest contribution for miRNA-7. MiR-7 and miR-409 are also a demonstrated case and strong candidate to undergo of TDMD, respectively (see main text).

C Boxplot showing the size of circRNAs (log2 of the base pairs) that interact with miRNAs from each of the different "sponging" quartiles. Shown are Wilcoxon rank sum test p-values (corrected with the Hochberg method for multiple comparisons) between the least sponged and the remaining groups (ns: $p > 0.05$).

D Barplot representing the percentages of overlapping genomic regions (CDS, 5'UTR, 3'UTR, etc) giving rise to the circRNAs with predicted binding sites against miRNAs within different quartiles of sponging suffered. No enrichment of genomics features for circRNAs interacting with miRNAs within the different quartiles was observed (Pearson's Chi-squared test p-value = 0.998).

Figure EV5.

Examples of predicted TDMD-like sites on circRNAs.

A-B Pie charts showing the proportion of and circRNA-miRNA (A) and linear RNA-miRNA (B) interactions involving at least one predicted TDMD-like site against miRNAs within quartiles of increasing "sponging suffered" coefficients. Shown are the p-values for the Fisher's Exact test between each quartile and the least sponged quartile ("- sponged").

C Examples of TDMD-like sites within circRNAs predicted and aligned using scanMiR. The five miRNAs belong to the "+++ sponged" quartile.

1115

Figure 1

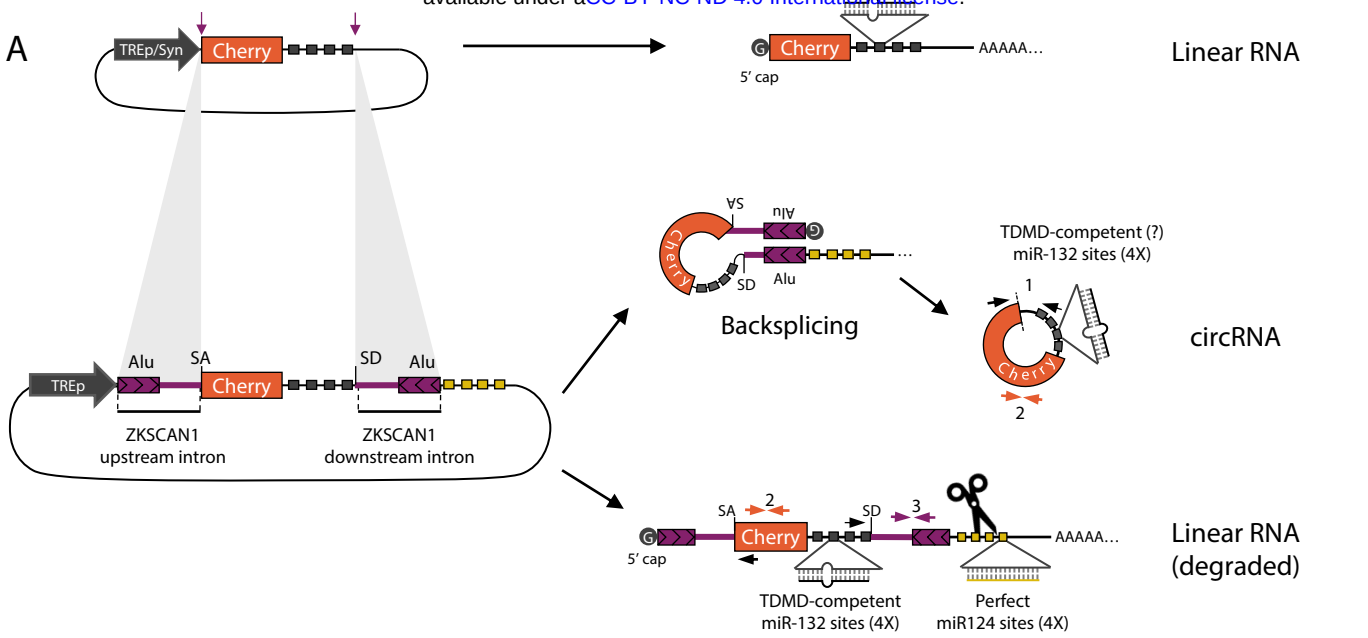

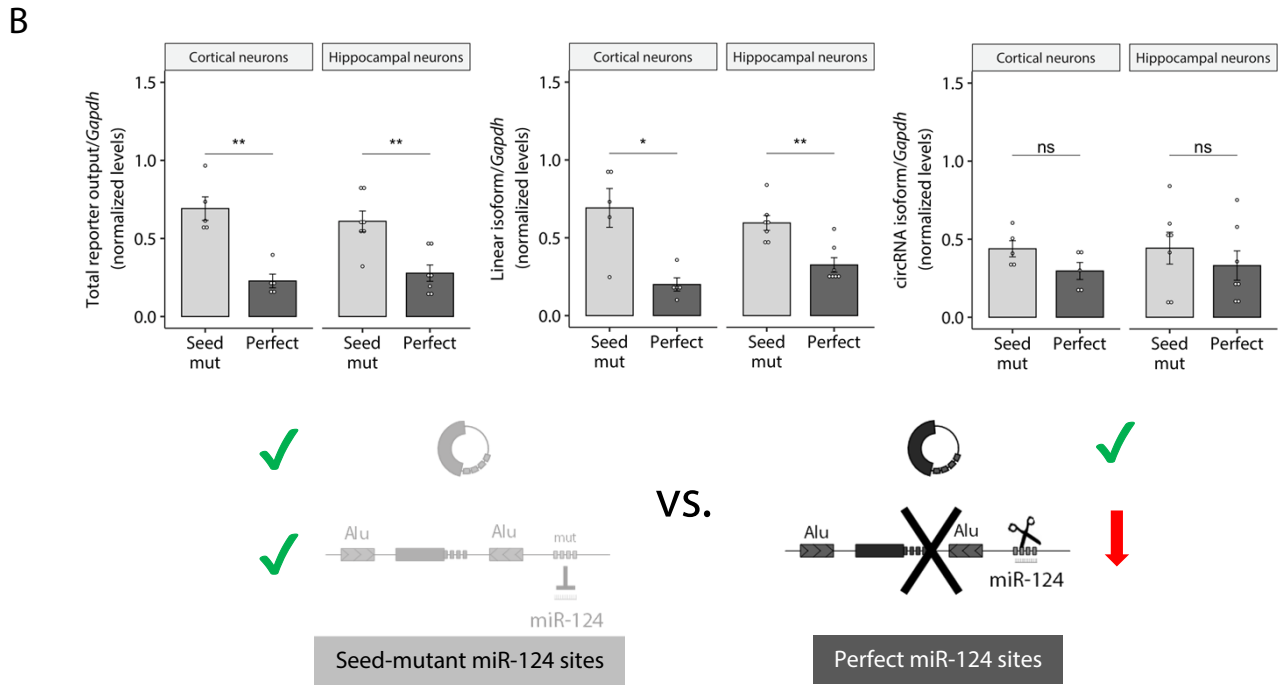

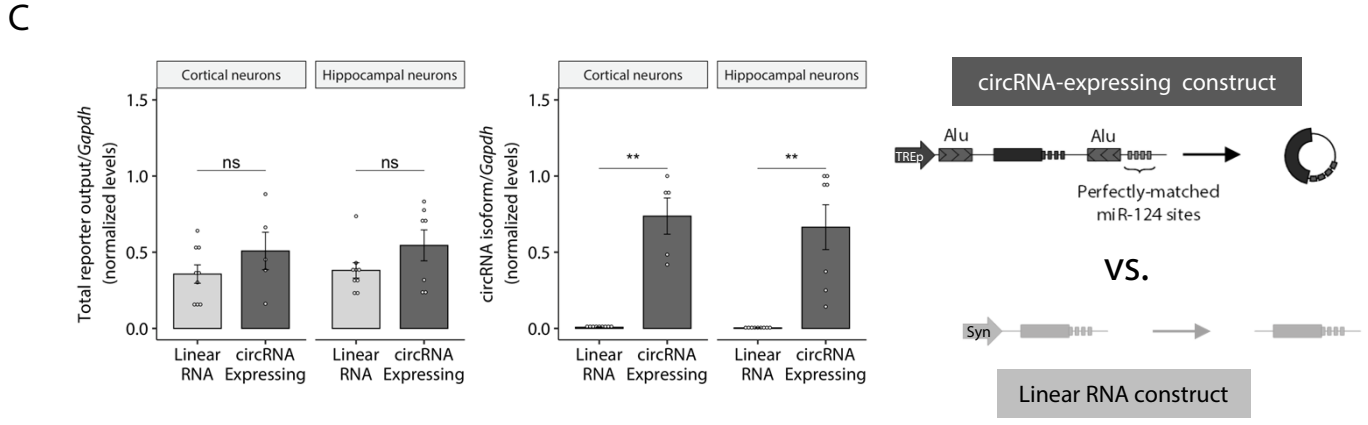

Figure 2

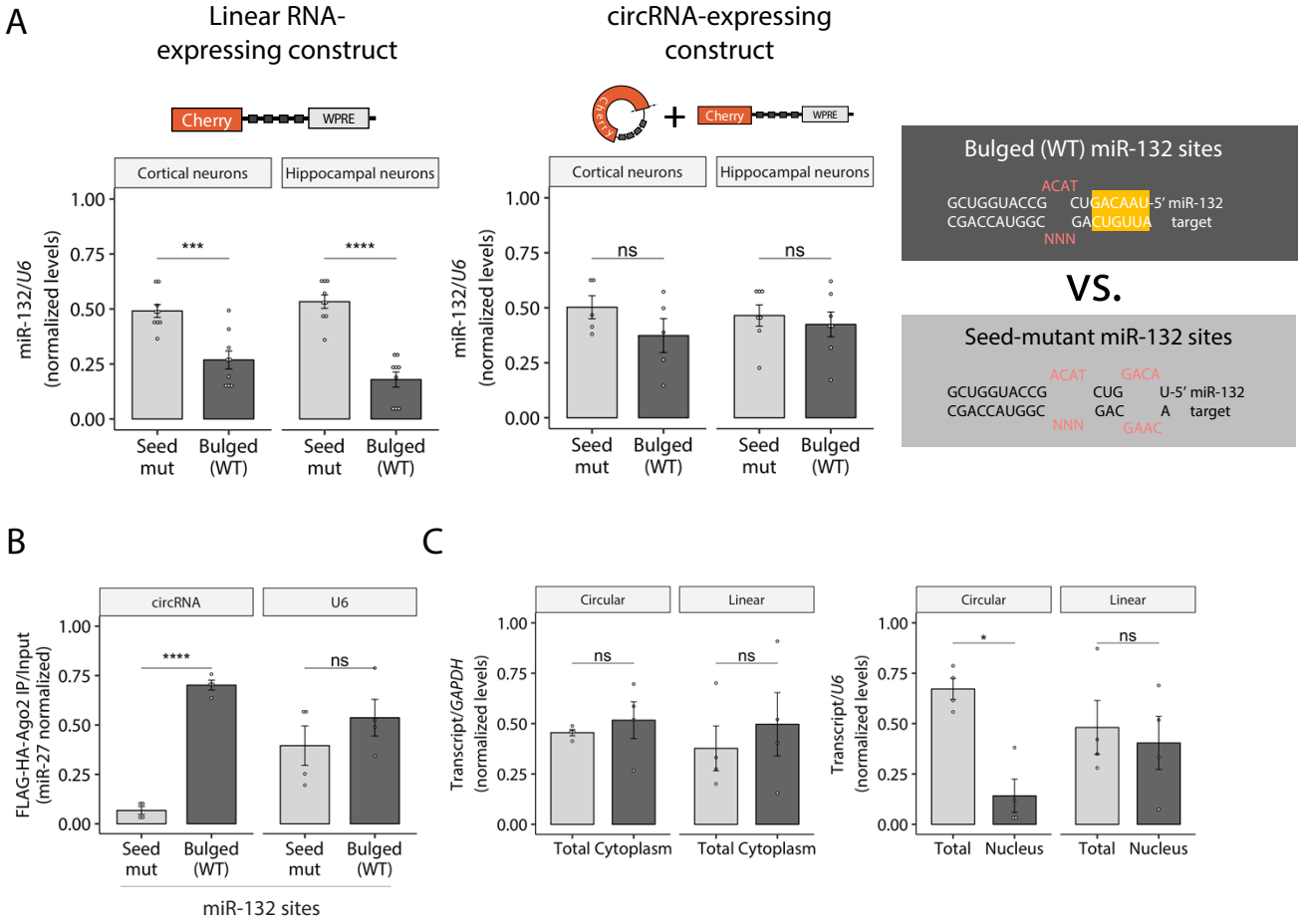

Figure 3

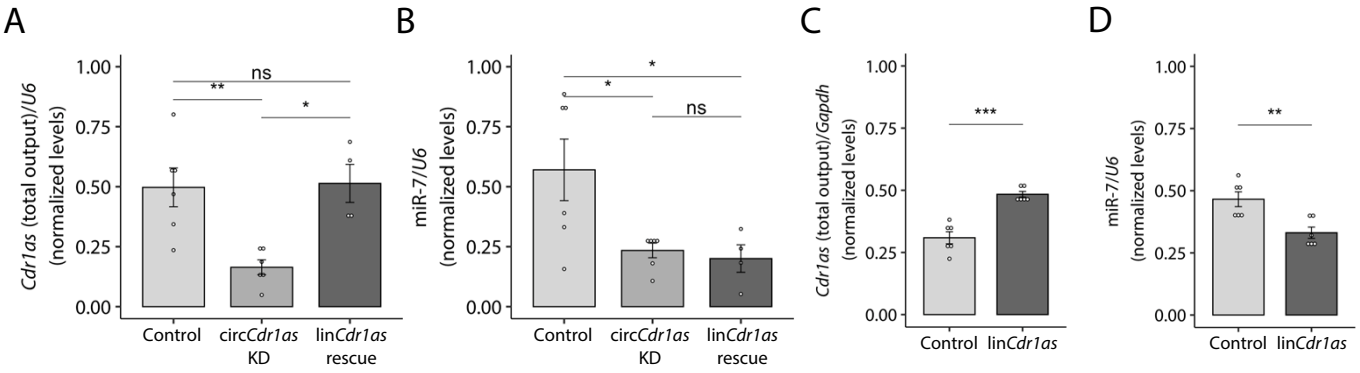

Figure 4

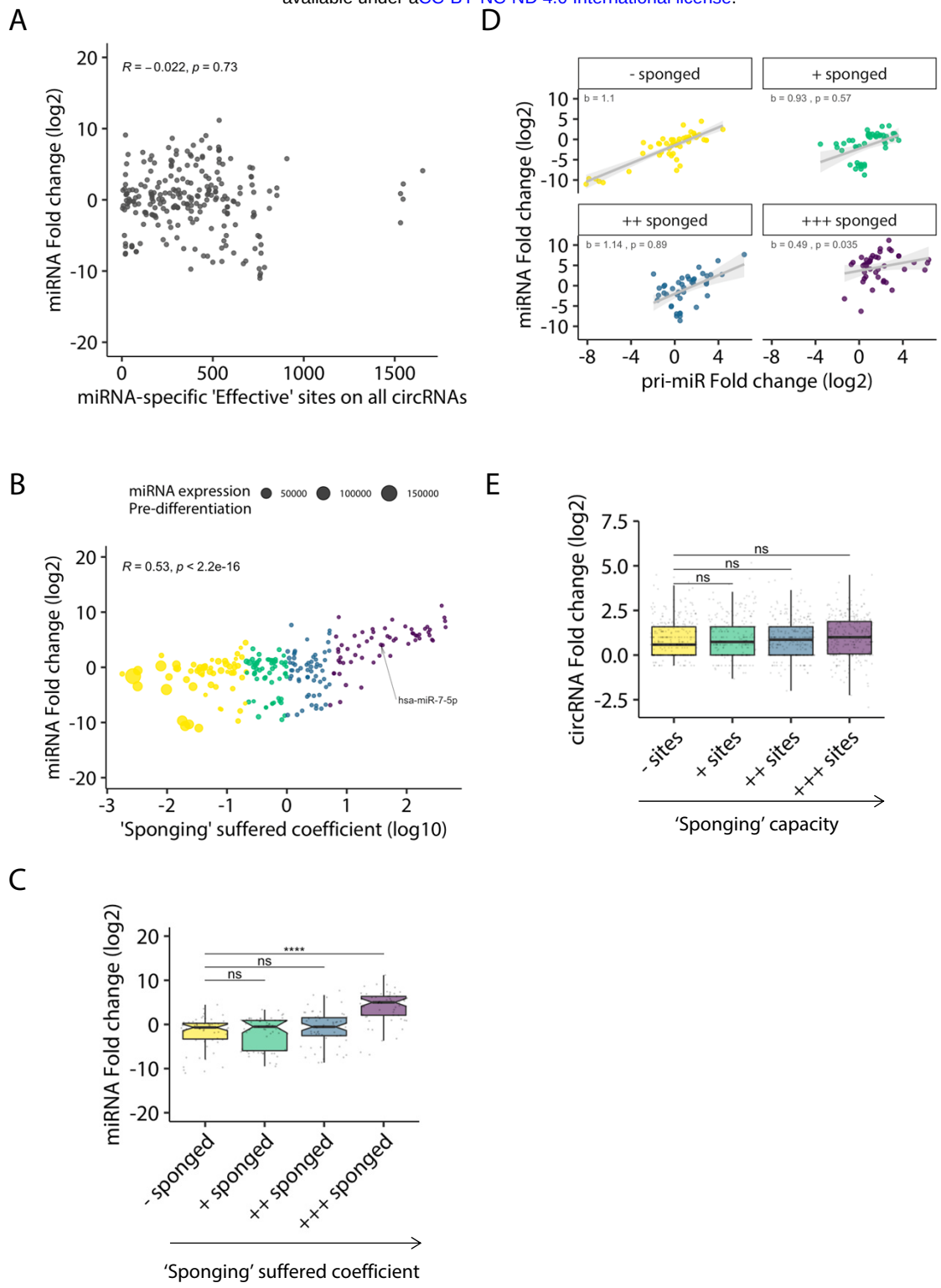

Figure 5

A

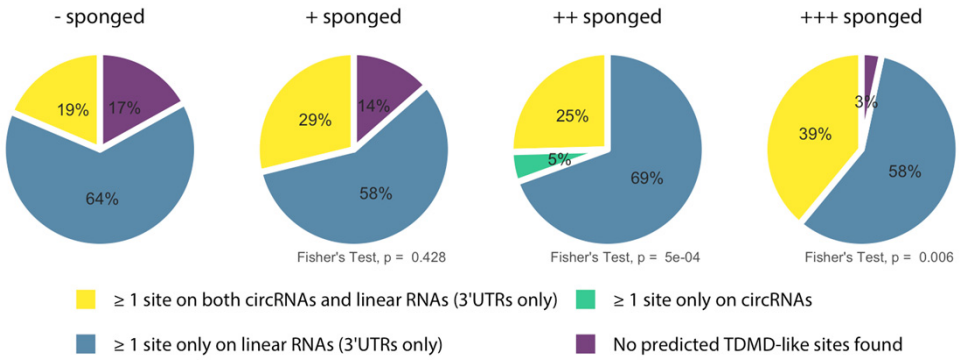

B